APL Materials

Suitability of binary oxides for molecular-beam epitaxy source materials: A comprehensive thermodynamic analysis

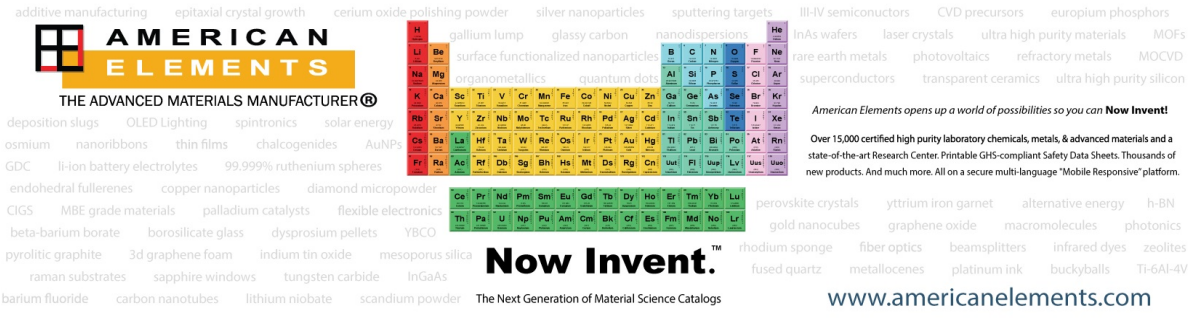
Cite as: APL Mater. **8**, 081110 (2020); https://doi.org/10.1063/5.0013159
Submitted: 08 May 2020 . Accepted: 06 August 2020 . Published Online: 24 August 2020

Kate M. Adkison, Shun-Li Shang, Brandon J. Bocklund, Detlef Klimm, Darrell G. Schlom, and Zi-Kui Liu

COLLECTIONS

This paper was selected as an Editor's Pick

View Online Export Citation CrossMark



© 2020 Author(s).

Suitability of binary oxides for molecular-beam epitaxy source materials: A comprehensive thermodynamic analysis

Cite as: APL Mater. 8, 081110 (2020); doi: 10.1063/5.0013159
Submitted: 8 May 2020 • Accepted: 6 August 2020 •
Published Online: 24 August 2020

View Online Export Citation CrossMark

Kate M. Adkison,[1] Shun-Li Shang,[1,a)] Brandon J. Bocklund,[1] Detlef Klimm,[2] Darrell G. Schlom,[2,3,4] and Zi-Kui Liu[1]

AFFILIATIONS

[1]Department of Materials Science and Engineering, The Pennsylvania State University, University Park, Pennsylvania 16802, USA
[2]Leibniz-Institut für Kristallzüchtung, Max-Born-Str. 2, 12489 Berlin, Germany
[3]Department of Materials Science and Engineering, Cornell University, Ithaca, New York 14853, USA
[4]Kavli Institute at Cornell for Nanoscale Science, Ithaca, New York 14853, USA

[a)]**Author to whom correspondence should be addressed:** sus26@psu.edu

ABSTRACT

We have conducted a comprehensive thermodynamic analysis of the volatility of 128 binary oxides to evaluate their suitability as source materials for oxide molecular-beam epitaxy (MBE). 16 solid or liquid oxides are identified that evaporate nearly congruently from stable oxide sources to gas species: As_2O_3, B_2O_3, BaO, MoO_3, OsO_4, P_2O_5, PbO, PuO_2, Rb_2O, Re_2O_7, Sb_2O_3, SeO_2, SnO, ThO_2, Tl_2O, and WO_3. An additional 24 oxides could provide molecular beams with dominant gas species of CeO, Cs_2O, DyO, ErO, Ga_2O, GdO, GeO, HfO, HoO, In_2O, LaO, LuO, NdO, PmO, PrO, PuO, ScO, SiO, SmO, TbO, Te_2O_2, U_2O_6, VO_2, and YO_2. The present findings are in close accord with available experimental results in the literature. For example, As_2O_3, B_2O_3, BaO, MoO_3, PbO, Sb_2O_3, and WO_3 are the only oxides in the ideal category that have been used in MBE. The remaining oxides deemed ideal for MBE awaiting experimental verification. We also consider two-phase mixtures as a route to achieve the desired congruent evaporation characteristic of an ideal MBE source. These include (Ga_2O_3 + Ga) to produce a molecular beam of Ga_2O(g), (GeO_2 + Ge) to produce GeO(g), (SiO_2 + Si) to produce SiO(g), (SnO_2 + Sn) to produce SnO(g), etc.; these suboxide sources enable suboxide MBE. Our analysis provides the vapor pressures of the gas species over the condensed phases of 128 binary oxides, which may be either solid or liquid depending on the melting temperature.

© 2020 Author(s). All article content, except where otherwise noted, is licensed under a Creative Commons Attribution (CC BY) license (http://creativecommons.org/licenses/by/4.0/). https://doi.org/10.1063/5.0013159

I. INTRODUCTION

Oxides are of enormous interest for a wide range of applications due to the useful behaviors they exhibit, often with property coefficients or figures of merit at or near the very highest. These include magnetoelectrics (e.g., Cr_2O_3),[1] ferroelectrics (e.g., $PbZr_{0.2}Ti_{0.8}O_3$),[2] ferromagnets (e.g., $La_{0.7}Sr_{0.3}MnO_3$),[3] ferrimagnets (e.g., Sr_2FeMoO_6 and $BaFe_{12}O_{19}$),[4,5] piezoelectrics (e.g., $PbZn_{1/3}Nb_{2/3}O_3$–$PbTiO_3$),[6] multiferroics (e.g., $BiFeO_3$),[7] superconductors (e.g., $HgBa_2Ca_2Cu_3O_{8+x}$),[8] metal-to-insulator transition materials (e.g., EuO),[9] and semiconductors (e.g., $BaSnO_3$[10,11] and CdO[12] with their high mobilities and Ga_2O_3[13,14] with its high figure of merit for power electronics).

To go from properties to technology, it is often desired to combine oxides with other materials to build and investigate the performance of proof-of-principle devices. One technique for producing high-quality oxides in thin film form is molecular-beam epitaxy (MBE). The resulting thin films can be used to establish the intrinsic properties of a material or assess its performance in prototype devices. MBE is widely employed for making high-quality thin films

© Author(s) 2020

because of its clean, ultra-high vacuum environment allowing film synthesis to be monitored by a variety of techniques during growth as well as its notable absence of highly energetic species. These characteristics allow for the precise customization of thin films with very few impurities and minimal disorder.[15] When it comes to preparing materials that are highly sensitive to crystalline perfection, MBE achieves electrical transport characteristics surpassing all other thin film growth methods, making it the gold-standard technique for preparing oxide heterostructures.[16–19]

MBE traditionally utilizes elemental molecular beams—one for each element in the compound being formed—that all impinge on the substrate to form the desired compound.[15] Challenges arise when this approach is applied to oxides. Consider trying to grow a layer of an oxide containing harder-to-oxidize elements on top of a layer that oxidizes easily and one does not want to overoxidize, as in the case for $SrTiO_3$/Si or $SrTiO_3$/$GdTiO_3$.[20,21] Having an increased variety of molecular beams to choose from, for example, ones that deliver species already oxidized, could enhance the ability to make well-controlled heterostructures involving oxides by MBE.

For multicomponent materials such as oxides, one might be tempted to just evaporate the desired oxide directly. In general, such an approach does not work because when most oxides are heated, they do not simply evaporate as molecules with the same composition as the starting material, i.e., congruently. Instead, some of the constituents have higher vapor pressures and evaporate first; they evaporate incongruently. This leads to the composition of what is left behind changing, resulting in the partial pressures of the species that evaporate from a multicomponent source to change over time, making it useless for the controlled deposition of thin films. There are, however, some well-known exceptions to this rule. For example, SiO is known to evaporate congruently in vacuum as SiO molecules.[22–24] However, how many other exceptions are there among oxides? Answering this question is important for experimentalists seeking suitable source materials for the growth of oxides by MBE.

Stolyarova and Semenov[22] summarized the gas species emanating from Knudsen cells containing many different binary oxides. Complete data, however, showing the partial pressure of each gas species as a function of temperature are not available for many of these oxides,[22] limiting the usefulness of the information for MBE experimentalists. Lamoreaux *et al.*[25,26] conducted thermodynamic analyses on the evaporation behavior of the oxides of elements in groups 1, 2, and 12–14 under reducing conditions (O_2 partial pressure, $P_{O_2} = 10^{-10}$ Pa), oxidizing conditions ($P_{O_2} = 2 \times 10^4$ Pa), and congruent evaporation conditions. By providing the partial pressures of the vapor species over the condensed oxides as a function of temperature, their results[25,26] are widely used to determine if an oxide will make a good MBE source material. Nonetheless, much of the periodic table remains to be filled in as data for many of the oxides of transition metals and rare-earth (*RE*) metals are missing from their studies.[25,26] This lack of knowledge motivates the present thermodynamic analyses in which we analyze the evaporation behavior of 128 binary oxides; see Table S1 in the supplementary material for a complete list.

In the present work, we perform thermodynamic calculations to comprehensively consider the suitability of binary oxides and two-phase mixtures as potential sources for oxide MBE. Most binary oxides are found to be unsuitable because upon heating, they decompose and evaporate a dominant species that contains either pure oxygen, which pollutes the vacuum environment, or the pure metal, which provides no benefit over using the pure metal directly. A few binary oxides are found that evaporate a metal oxide molecule in the vapor phase and are thus suitable for oxide MBE. Some of these are well appreciated and utilized, while others are new and await experimental verification. Several two-phase mixtures are also found to be suitable for oxide MBE.

II. METHODOLOGY

A. Thermodynamic analysis of evaporation for oxides

Equilibrium calculations were performed using the SGTE substance database (SSUB5)[27] within the Thermo-Calc software[28] to assess the evaporation behavior of binary oxides, i.e., the gaseous species and their vapor pressures. For amorphous SiO(am), which is well-known to evaporate congruently,[22–24] its close chemical relative GeO(am), and compounds including PtO_2, Pt_3O_4, and PtO, which are missing in the SSUB5 database, thermodynamic descriptions were added using the reported enthalpies (and entropies when available) of formation at 298.15 K for GeO(am),[29] SiO(am),[30] and the Pt–O compounds.[31] In calculating the evaporation behavior of oxides, the gas species with the highest partial pressure—which with the increasing temperature is the first to reach a vapor pressure of 10^{-1} Pa—is described as the "dominant" species. The relevance of 10^{-1} Pa for MBE is that this partial pressure at the source is typically used for thin film growth.[32–34] If two gas-phase species have the same concentration within a factor of 10, they are both considered dominant; this is the case for the binary oxides of CsO_2, PbO, Rb_2O, Sc_2O_3, TcO_2, U_4O_9, and ZrO_2.

In thermodynamic calculations, the components of the system are defined as the element of interest and O_2 with the number of moles of the non-oxygen element fixed to one, i.e., $n(M) = 1$ mol. It is worth mentioning that there are many oxygen-containing species in the gas phase such as O, O_2, and O_3. At equilibrium, there is only one independent partial pressure for the independent component O, which can be represented by P_{O_2}, or P_O, or P_{O_3}, or the partial pressure of any O-containing species, and the partial pressures of other O-containing species are dependent variables and can be calculated. In other words, the number of independent partial pressures (or activity or chemical potential) equals the number of independent components in the system, and the partial pressures of other components (species) can be calculated, but they are not independent.

The partial pressure of O_2 is fixed at 10^{-4} Pa, a typical oxygen background pressure in the growth of oxides by MBE, because at higher background pressures, hot filaments and other MBE components are damaged from oxidation and the fluxes from many elemental sources become unstable due to surface oxidation.[35,36] Calculations are made with the gas phase fixed at zero amount as this is considered to represent equilibrium evaporation from an MBE source; when the material evaporates from an MBE source into the open system of MBE, it does not return. It is worth noting that the total pressure in the system equals the vapor pressure of the condensed phases, which varies with temperature in equilibrium with

© Author(s) 2020

the fixed gas phase and should not be set as a fixed equilibrium condition in thermodynamic calculations. Furthermore, another benefit in using the partial pressure of O_2 as a fixed equilibrium condition is that the oxygen content in the system is self-regulated by the phase stability of the system. This is an open system with respect to O_2, and the amount of O_2 not only is different in different systems but also varies in the same system as the temperature is changed. An example of the macro file (i.e., the tcm file used by the Thermo-Calc software) to calculate the evaporation of a stable oxide source is provided in Table S3 in the supplementary material.

For metastable oxides in equilibrium with gas, the gas compositions are calculated under the same conditions (temperature, O_2 activity, and moles of the element) as those used for the stable oxide sources, but with all condensed phases removed except for the metastable oxide of interest. Two scenarios are possible when the oxide decomposes; these depend on the kinetics of the compound. If the solid oxide decomposes faster into a metal-oxygen containing gas phase than into another oxide or metal condensed phase, the metastable oxide is potentially useful as an oxide MBE source. If, on the other hand, the solid oxide decomposes faster into another condensed phase (oxide or pure element), O_2 gas will be produced and pollute the vacuum. An example of the macro file to calculate the evaporation of a metastable oxide source is provided in Table S3 in the supplementary material.

For the cases of gas species evaporated from a two-phase mixture of M_mO_n + M with an overall composition M_xO_y, the conditions for thermodynamic calculations are $n(M) = 1$ mol, $n(O_2) = 0.5y/x$ mol, and the amount of gas phase is fixed at zero, while the partial pressure of O_2 is determined by the three-phase equilibrium of the two condensed phases and the gas phase. The pressure of the gas phase is much lower than the 10^{-4} Pa typical oxygen background pressure used in the growth of oxides by MBE that is mentioned above due to the presence of the pure metal in equilibrium at low temperatures. Nevertheless, when the pure metal becomes metastable at high temperatures, the partial pressure of O_2 can increase significantly as shown in the discussion of Ga_2O_3 and relevant to suboxide-MBE (S-MBE). An example of the macro file to calculate the evaporation of a two-phase mixture case is provided in Table S3 in the supplementary material.

These two types of calculations, i.e., the cases with the fixed partial pressure of O_2 vs the two-phase mixture, represent the two different thermodynamic constraints on the system, viz., an open system vs a closed system. Even though the MBE chamber is an open system, in practice because gas is exchanged between the MBE chamber and the surroundings via the input of gases and its departure through several vacuum pumps, it can behave like either an open or a closed system depending on the fluxes of metallic elements, the partial pressure of O_2, and temperature as demonstrated in the discussion of the thermodynamics of MBE (TOMBE) diagram for ternary systems.[19] In the TOMBE diagram, O_2 partial pressure is plotted against temperature and the diagram is labeled with the stable phases with the gas phase always present. For a binary system, in the closed-system regions of the TOMBE diagram, two condensed phases and the gas phase are in equilibrium with one degree of freedom (independent number of potentials) based on the Gibbs phase rule.[37] This is the same situation as typical Ellingham diagrams, such as the two-phase mixture in the present work of two components, with the temperature being the independent potential and the chemical potentials being dependent potentials. Meanwhile in the open-system regions, one condensed phase and the gas phase are in equilibrium with two degrees of freedom. This is the case for a fixed partial pressure of the non-oxygen element with both the temperature and the chemical potential of O_2 being independent potentials in maintaining the two-phase equilibrium. For evaporation, both scenarios are useful as demonstrated in the present work, while for MBE growth of thin films, the open-system scenario with one condensed phase is ideal as demonstrated in the MBE growth of Sr_2RuO_4, $SrRuO_3$, and $CaRuO_3$ epitaxial films.[17,19]

B. Five scenarios of oxide source evaporation

Four possible scenarios for the evaporation of oxide sources are shown in Fig. 1. These are each described in detail below, together with one additional possibility (scenario 5) consisting of the evaporation of mixtures of two condensed phases. Note that we ignore the complex reaction products in scenarios 2–4 for the sake of simplicity; for example, we ignore the possible products of new oxide + O_2, or new oxide + M, or new oxide + additional oxide, or any combination of them other than the mentioned product M_mO_n.

Scenario 1: Nearly congruent evaporation of metal-oxygen gas species [M_xO_y(s or ℓ) → M_xO_y(g); see S1 of Fig. 1]. Here, the letters s, ℓ, and g in the parentheses indicate solid, liquid, and gas phases, respectively. In congruent evaporation, the species that evaporates into the gas phase has the same stoichiometric ratio as the solid or liquid source from which it comes; see additional details in Sec. II C. Two attributes make congruent evaporation the best scenario for MBE sources: (i) when the oxide is heated in the crucible and evaporates, metal-oxygen containing gas species of known composition will traverse the MBE chamber and deposit onto the substrate, and (ii) the metal-oxygen gas species M_xO_y(g) has the same stoichiometric ratio as the source material M_xO_y(s or ℓ), so the composition of the source material will remain constant over time, making it easier to provide a stable flux of this molecular beam of known composition.

Scenario 2: Incongruent evaporation of metal-oxygen gas species [M_xO_y(s or ℓ) → M_mO_n(g); see S2 of Fig. 1]. In incongruent evaporation, the species that evaporate have a different

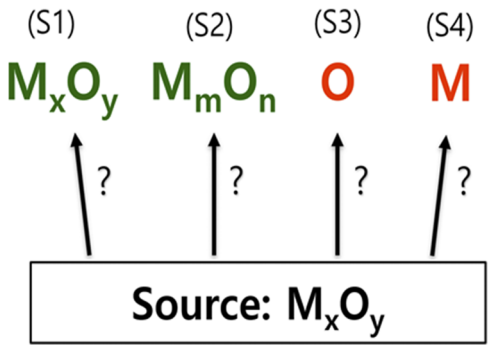


FIG. 1. Four scenarios (S1–S4) possible during evaporation plus an additional scenario (S5) examined in the present work with a two-phase mixture of M_xO_y + M as a source. Note that this plot ignores the possibility of complex reaction products that form from the oxide source for the sake of simplicity.

© Author(s) 2020

overall stoichiometric ratio than the solid or liquid source from which they emanate. Like congruent evaporation, incongruent evaporation can work for the MBE process, but it is less ideal. Although metal-oxygen containing gas species will be deposited onto the substrate, the gas species coming off of the oxide source [M_mO_n(g)] has a different stoichiometric ratio than the source [M_xO_y(s or ℓ)]. This difference in chemistry will cause the source material composition to change over time, making it more difficult to control the flux and composition of the molecular beam.

Scenario 3: Evaporation of oxygen species [M_xO_y(s or ℓ) → O_z(g); see S3 of Fig. 1]. For some oxides, oxygen species [O_z(g)] will be the dominant species in the vapor. The dominant evaporation of oxygen species from the metal-oxide source is undesirable for an MBE process. In oxide MBE, it is desired to control the oxidant species (often an activated species such as ozone or those emitted from an oxygen plasma) and its flux directly. Oxygen species [O_z(g)] coming from the metal-oxide sources effectively pollute the ultra-high vacuum and cause a loss of the independent control of growth parameters that is desired in MBE.

Scenario 4: Evaporation of elemental metal species [M_xO_y(s or ℓ) → M_z(g); see S4 of Fig. 1]. An elemental metal [M_z(g)] can also be the dominant species given off by the oxide source. Oxides that evaporate elemental metal species are also undesirable for MBE. Evaporation of the elemental metal causes the oxide source composition to become oxygen rich over time. In addition, using such an oxide source to generate a flux of metal species generally offers no advantage over the use of a pure metal source.

Scenario 5: Two-phase mixture of M_mO_n + M as sources. In addition to the above four scenarios, we also examine one more scenario to produce gas species M_xO_y from a two-phase mixture M_mO_n + M with an overall composition M_xO_y. This scenario builds upon experimental work, showing that this is a viable approach.[38,39]

C. Three criteria for a nearly ideal MBE source material

Once the gas compositions emanating from the binary oxides are calculated, each binary oxide is evaluated against three criteria based on MBE chamber conditions necessary to produce high-quality thin films. A binary oxide source is identified as the most ideal for oxide MBE if it meets all three of the following criteria:

Criterion 1. The solid or liquid metal-oxide source is stable under the given conditions. Stable metal-oxide sources are ideal because they do not decompose and release oxygen, which would pollute the MBE vacuum. Some elements in the SSUB5 database[27] such as actinium, astatine, californium, curium, einsteinium, fermium, francium, radium, and protactinium do not have solid or liquid oxides, so these are disqualified. Oxides of some transition metal are disqualified because the stable phase under the given conditions is a pure metal in solid or liquid form. Examples include Ag(s), Au(ℓ), Co(s), Cu(s), Ir(s), Os(s), Pd(s), Rh(s), and Ru(s). A select few of the elements are stable as liquid oxides under the given conditions such as Bi_2O_3(ℓ), FeO(ℓ) (i.e., the liquid Fe-oxide phase or the slag phase), Nb_2O_5(ℓ), Rb_2O(ℓ), Ta_2O_5(ℓ), and Ti_4O_7(ℓ). If an element is able to form a metastable oxide, the metastable oxide is investigated. For example, Ir(s) is the most stable phase under the given conditions, but iridium also forms IrO_2. Hence, IrO_2 is investigated as a metastable source. Note that the liquid state of FeO(ℓ) is a slag phase with a mixture of all iron oxides (such as FeO, Fe_3O_4, and Fe_2O_3) in arbitrary ratios. Usually, melting processes are accompanied by a change in the metal-oxygen stoichiometry to lower the Gibbs energy by mixing, but not in the solid state.

Criterion 2. The oxygen-metal containing gas species is dominant. A metal-oxygen gas species [M_xO_y(g)] is ideal as it provides pre-oxidized metals with the known oxygen content to the growing film when it reaches the substrate. Binary oxides for which the dominant evaporant is the oxygen species or metal species are disqualified as MBE sources for not meeting this second criterion.

Criterion 3. The oxide source evaporates nearly congruently. Congruent evaporation ensures that the oxide source provides a constant flux of the desired species at a fixed temperature. This third criterion distinguishes between the most ideal sources for MBE and those that are less ideal because they evaporate incongruently.

Note that for exact congruent evaporation, the composition of the source oxide (solid or liquid phase) and that of the gas phase evaporating from it must be identical. The ideal case is where only one species exists in the gas phase and that species has the same stoichiometric ratio as the solid or liquid MBE source from which it evaporated. This is rarely the case; usually, multiple species evaporate into the gas phase, and congruent evaporation occurs when the overall composition of the gas phase matches that of the solid or liquid MBE source from which it came. As a practical matter, exact congruent evaporation is not needed for a source to perform well in MBE. Sources with evaporation characteristics sufficiently close to exact congruent evaporation can be tolerated. In the present work, we define nearly congruent evaporation as the condition where the mole fraction difference for each component, such as O_2, in the oxide source and in the gas phase is less than 0.01, i.e., $|\Delta x(O_2)| < 0.01$, with

$$\Delta x(O_2) = x(\text{oxide}, O_2) - x(\text{gas}, O_2), \tag{1}$$

where $x(\text{oxide}, O_2)$ and $x(\text{gas}, O_2)$ are the mole fractions of the component O_2 in the oxide source (s or ℓ) and in the gas phase, respectively. The same condition is also used to define what we mean by the nearly congruent evaporation of metastable oxide sources.

III. RESULTS AND DISCUSSION

In the SSUB5 database,[27] 58 elements have stable solid oxides and 14 elements have metastable oxides under the given conditions. To make the present study more comprehensive, additional metastable oxides under the given conditions are included. The list of all evaluated 128 stable and metastable oxides and 17 elements under the given conditions is available in Table S1 in the supplementary material. In addition, 27 two-phase mixtures of M_mO_n + M

© Author(s) 2020

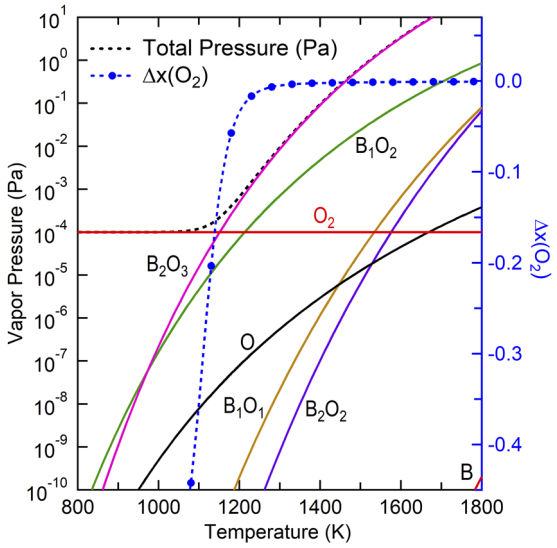


FIG. 2. Calculated partial pressures of the species in the gas phase (the solid lines) over the stable solid B_2O_3 (the amorphous/glass phase) source at a fixed oxygen partial pressure, P_{O_2} = 10^{-4} Pa. The dominant gas species possesses the same composition as the B_2O_3(s) source at T > 1160 K. Nearly congruent evaporation of B_2O_3(s) occurs at T > 1255 K [see the definition in Eq. (1)]. If the total pressure is fixed at P_{tot} = 0.1 Pa, instead of P_{O_2} being fixed at 10^{-4} Pa, then nearly congruent evaporation of B_2O_3(s) occurs at T > 1398 K; see also the summary in Table I.

are examined, where the elements M considered are rare-earth elements and other elements of practical interest; see Table S2. Note that we do not plot phase stability as a function of temperature for these oxides. Instead, we note in Figs. 2 and 4 and each supplemental figure caption (Figs. S1-S81) the stable phases as a function of temperature for each system.

A. Ideal MBE sources

16 solid and liquid oxides meet the criteria to be classified as ideal MBE sources. These are As_2O_3, B_2O_3, BaO, MoO_3, OsO_4, P_2O_5, PbO, PuO_2, Rb_2O, Re_2O_7, Sb_2O_3, SeO_2, SnO, ThO_2, Tl_2O, and WO_3; see Table I. Some of these oxides have been well studied in Knudsen cell evaporation experiments. Some of the identified oxide sources have been used to make thin films via various deposition methods, but only As_2O_3, B_2O_3, MoO_3, PbO, Sb_2O_3, SeO_2, and WO_3 have been used successfully for MBE growth as described in below. We discuss these oxides in Secs. III A 1–III A 13 in alphabetical order except for As_2O_3 and SnO, which are discussed with Sb_2O_3 in Sec. III A 9, and PuO_2, which is discussed with ThO_2 in Sec. III A 11.

1. B_2O_3(s) (Fig. 2)

Figure 2 shows the calculated evaporation behavior of solid B_2O_3 (the amorphous/glass phase) as a function of temperature under P_{O_2} = 10^{-4} Pa, where the B_2O_3 gas species is dominant above 1160 K in equilibrium with solid B_2O_3(s); see also Table I.

TABLE I. Oxide sources (s or ℓ) meeting the criteria for an ideal MBE source under the following conditions: P_{O_2} = 10^{-4} Pa, fixed gas phase at zero amount, fixed T, and $n(M)$ = 1 mol.

Element	Oxide source	Dominant gas species	T-range[a]	T-range[b]	T-range[c]
As	As_2O_3(ℓ)	As_4O_6	>677	>611	650–1274[d]
B	B_2O_3_glass(s)	B_2O_3	700–1800	1160–1800 (O_2 at T < 1160)	1255–1800
Ba	BaO(s)	BaO	700–1800	>1330 (O_2 at T < 1330)	>1473
Mo	MoO_3(s)	Mo_3O_9; Mo_4O_{12}	700–1800	760–1800 (O_2 at T < 760)	768–1800
Os	OsO_4(s, ℓ)	OsO_4	<314	<314	<314
P	P_2O_5_orth(s, ℓ)	P_4O_{10}	s at 300–839; ℓ at T > 839	422–1552 (O_2 at T < 422)	438–1510
Pb	PbO_yellow(s)	PbO	700–1162	848–1032 (Pb at T > 1032)	905–918
Pu	PuO_2(s)	PuO_2	700–2200	1850–2200 (O at T < 1850)	1999–2063
Rb	Rb_2O(s, ℓ)	Rb_2O; Rb	s at 517–778; ℓ at T > 778	660–795 (O_2 at T < 660)	701–716
Re	Re_2O_7(s, ℓ)	Re_2O_7	s at 300–600; ℓ at T > 600	320–1286 (O_2 at T < 320)	332–1244
Sb	Sb_2O_3(ℓ)	Sb_4O_6	>997	997–1429	997–1383
Se	SeO_2(s, ℓ)	SeO_2	s at 300–633; ℓ at T > 633	314–650 (O_2 at T < 314)	337–644
Sn	SnO(ℓ)	SnO	>1498	1498–1800 (O_2 at T < 863)	1498–1756
Th	ThO_2(s)	ThO_2	700–3000	2440–2970 (O at T < 2440 and ThO at T > 2970)	2631–2720
Tl	Tl_2O(s, ℓ)	Tl_2O	s at 650–852; ℓ at T > 852	650–1456 (Tl at T > 1456)	650–1188
W	WO_3(s)	W_3O_9	700–1800	1150–1800 (O_2 at T < 1150)	1176–1800

[a]Temperature range (in K) where the oxide source (s or ℓ) is stable.
[b]Temperature range (in K) where the dominant gas species possesses the same composition as the binary oxide source from which it evaporates.
[c]Temperature range (in K) of nearly congruent evaporation as defined by Eq. (1) for an absolute value of $\Delta x(O_2)$ < 0.01. Note that some high-temperature limits represent the selected temperature limits used in the present work to perform thermodynamic calculations; for example, 1800 K is the limit of our calculations rather than the limit of nearly congruent evaporation.
[d]Liquid As_2O_3 is stable at T > 677 K. The temperature range for nearly congruent evaporation from a stable source is 677 K–1274 K.

© Author(s) 2020

Figure 2 shows that nearly congruent evaporation of B_2O_3(s), defined by $|\Delta x(O_2)| < 0.01$ [see Eq. (1)], occurs at $T > 1255$ K. As an ancillary test, the ideal congruent evaporation of B_2O_3(s) occurs at $T > 1398$ K under a fixed total pressure, $P_{tot} = 0.1$ Pa. The thermodynamics of B_2O_3(s) volatility was investigated by Lamoreaux *et al.*,[26] and it was shown to evaporate congruently as B_2O_3(g). Stolyarova and Semenov[22] also noted that the dominant vapor species of B_2O_3(s) thermally evaporated by a Knudsen cell is B_2O_3(g). B_2O_3 sources in MBE are well known, though they have only been used as doping sources for the MBE growth of silicon.[40,41]

Although B_2O_3 is ideal for oxide MBE (see Fig. 2), and thin films have been successfully fabricated using MBE, the high reactivity of B_2O_3 with water to form H_3BO_3 under ambient conditions precludes it from many practical applications.[42] Putkonen and Niinistö[42] applied a protective Al_2O_3 capping layer using atomic layer deposition (ALD) to prevent the B_2O_3 thin film from reacting. When patterned, however, the film immediately suffered degradation from the exposed B_2O_3 edge. Proposed applications of B_2O_3 thin films include transistors, ultra-wide bandgap amorphous oxide semiconductors, and optoelectronics when combined with other oxides.[43–45] Glassy thin films such as B_2O_3 also have potential as electrolytes used in batteries, as electrochemical sensors, as supercapacitors, and as electrochromic sensors.[45]

2. BaO(s) (Fig. S8)

The calculated evaporation behavior of BaO is shown in Fig. S8 along with that of BaO_2; see also Table I. It can be seen that the primary species evaporating from BaO_2 is BaO, so a BaO_2 source works the same as BaO. The dominant BaO species in the molecular beam is relevant to making high dielectric constant perovskites such as $BaTiO_3$ and (Ba, Sr)TiO_3, which have applications in high-K (K is the dielectric constant) memory,[46] tunable dielectrics,[47,48] optoelectronics,[49–51] and fuel cells.[52,53] Another important barium-containing oxide is $BaSnO_3$—a semiconductor with high mobility at room temperature—which offers tantalizing properties for transparent electronics.[10,11,54,55] Barium hexaferrites including $BaFe_{12}O_{19}$ are ferrimagnetic insulators with excellent performance at high frequency.[5,56–58]

In addition to complex oxides containing barium, BaO thin films themselves have applications in high current density cathodes, thermionic energy converters, and optical devices.[59] BaO films have been grown by many groups using MBE with separate beams of barium and O_2.[60–62] Less common, but nonetheless demonstrated, is the growth of BaO films using a BaO_2 source[63] or a BaO source.[64,65] A BaO source could prove particularly advantageous when it is desired to not introduce any excess oxygen, e.g., when growing BaO on silicon and it is ideal to have all of the barium oxidized, yet not to oxidize any of the silicon (which can easily occur if excess oxygen is present).[61,62]

3. MoO_3(s) (Fig. S41)

Several studies have been carried out on the evaporation of MoO_3 from a Knudsen cell. In these studies, $(MoO_3)_3$, $(MoO_3)_4$, and $(MoO_3)_5$ are all observed in the gas phase with $(MoO_3)_3$ being most abundant at 850 K.[66,67] Our calculations (Fig. S41, see also Table I) indicate congruent evaporation of MoO_3 as well ($T > 768$ K at $P_{O_2} = 10^{-4}$ Pa) also with Mo_3O_9 and Mo_4O_{12} being most dominant followed by Mo_5O_{15}. Du *et al.*[68] grew MoO_3 thin films by MBE on $SrTiO_3$ substrates by evaporating MoO_3 powder from an effusion cell onto a substrate held at 673 K–823 K and immersed in activated oxygen species from an oxygen plasma operating at $P_{O_2} = 4 \times 10^{-4}$ Pa. MoO_3 molecular beams could be used as a route to grow $SrMoO_3$ thin films, which are being studied for use as transparent conductors because of their very high conductivity.[69,70] MoO_3 thin films are also used as electrochromic sensors and in lithium batteries.[71]

4. OsO_4(s, ℓ) (Fig. S48)

Solid OsO_4(s) is a stable phase at low temperature, $T < 304$ K. With the increasing temperature, liquid OsO_4(ℓ) becomes stable in a narrow temperature range from 304 K to 314 K. Above 314 K, OsO_2(s) is the stable phase and remains so up to 832 K where solid Os(s) becomes stable. Figure S48 shows that the dominant gas species is OsO_4(g) at low temperatures, i.e., $T < 1028$ K in the plot of OsO_2(s) as an oxide source as well as in the plot of OsO_4(s) as an oxide source. These results indicate that OsO_4(s, ℓ) is an ideal source for MBE oxide when $T < 314$ K at $P_{O_2} = 10^{-4}$ Pa; see also Table I.

5. P_2O_5(s, ℓ) (Fig. S47)

The calculated evaporation behavior of solid P_2O_5 with an orthorhombic structure is shown in Fig. S47; see also the data in Table I. P_2O_5 has exciting uses as a bioactive thin film material to modify surface properties of biomedical devices, to increase corrosion resistance, or for osteogenic applications.[72] The P_2O_5 thin films are commonly fabricated using a sol–gel method instead of physical vapor deposition. Stolyarova and Semenov[22] recorded the congruent evaporation of P_4O_{10} to P_4O_{10} gas species from a P_2O_5(s) source at 500 K. No publication in the literature was found using P_2O_5 in an MBE process.

6. PbO(s) (Fig. S50)

PbO(s) was shown by Lamoreaux *et al.*[26] to have dominant species Pb(g) under reducing conditions and PbO(g) under oxidizing conditions. Experiments by Lopatin *et al.*[73] found that the dominant gas species in PbO(s) evaporated at 900 K–1150 K are Pb_nO_n(g), Pb(g), and O(g). The Pb_nO_n(g) species comes from the congruent evaporation of nPbO(s) → Pb_nO_n with n = 1–6; the Pb(g) and O(g) species come from a partial dissociation of PbO(s) → Pb(g) + $\frac{1}{2}O_2$. The polymeric Pb_nO_n gas species observed by Lopatin *et al.*[73] were also included in the evaporation analysis by Lamoreaux *et al.*,[26] but these Pb_nO_n gas species are not included in the SSUB5 database and can thus not be seen in Fig. S50. Although the present work does not take into account the Pb_nO_n (n = 2–6) species, the yellow orthorhombic phase PbO_yellow is dominant below 1163 K under the conditions of our thermodynamic calculations (not shown), which agrees with Lopatin's assessment that PbO is dominant between 900 K and 1150 K.

The evaporation behavior of PbO_yellow in Fig. S50 disagrees with the analysis by Lamoreaux *et al.*,[26] which shows Pb(g) to be dominant from 700 K to 1800 K at $P_{O_2} = 10^{-10}$ Pa. On the other hand, an experimental attempt at using PbO(s) as an MBE source in an MBE system with no added oxygen (and a chamber background pressure in the 10^{-10} Pa range) found that PbO(s) decomposed into mainly Pb(g) with very little PbO(g),[74] which is consistent with

© Author(s) 2020

the expectations of Lamoreaux *et al.*[26] To see if the disagreement between our calculations and those of Lamoreaux *et al.*[26] is due to the difference in O_2 partial pressure conditions, we redid our calculations as a function of oxygen partial pressure for P_{O_2} from 10^{-1} Pa to 10^{-10} Pa. Figure 3 shows the temperatures at which Pb(g) becomes the dominant species in the gas phase as a function of P_{O_2}; the temperature at which Pb(g) becomes dominant over PbO(g) decreases with decreasing P_{O_2}. At the pressure used by Lamoreaux *et al.*,[26] P_{O_2} = 10^{-10} Pa, the calculations show that the partial pressure of Pb(g) exceeds that of PbO(g) at 725 K, in good agreement with findings of Lamoreaux *et al.*[26] who found that this crossover occurs around 700 K at P_{O_2} = 10^{-10} Pa.

A PbO source was used by Rispens and Noheda to grow high-quality $PbTiO_3$ films by MBE.[75] These authors found the use of PbO(s) advantageous over Pb(ℓ), which is consistent with the results from Fig. S50 where the dominant species in the gas phase at MBE-relevant growth conditions is PbO. We note that based on the diagram by Lamoreaux *et al.*,[26] PbO is not a good source to use for the growth of $PbTiO_3$ or other Pb-containing oxides by MBE. This points to the importance of the current comprehensive analysis at a fixed oxygen pressure (10^{-4} Pa) that is relevant for oxide MBE and in the case of PbO dramatically changes the dominant species in the gas phase as shown in Fig. 3.

7. Rb_2O(s, ℓ) (Fig. S56)

Rb_2O is a liquid at temperatures at which the dominant species evaporated from it have a vapor pressure of 10^{-1} Pa. At this temperature, there are actually two species with high and comparable vapor pressure in the gas phase: Rb(g) and Rb_2O(g). From the calculated vapor pressures over liquid Rb_2O, Rb_2O is seen to evaporate nearly congruently at higher partial pressures of O_2 (such as P_{O_2} = 10^{-4} Pa and 10^{-1} Pa); see Fig. S56 as well as Table I.

At lower P_{O_2} (e.g., <10^{-4} Pa), the vapor is Rb-rich compared to the Rb_2O source. Although at these lower oxygen partial pressures it is not an ideal MBE source, it should still produce a molecular beam containing a significant fraction of pre-oxidized rubidium in the form of Rb_2O. Rb_2O has been used as an MBE source for the growth of superconducting (Bi, Rb)BaO_3 films by Hellman *et al.*[76] These authors noted that the Rb_2O source showed signs of decomposition into a Rb-rich molecular beam, consistent with the present calculations at different P_{O_2} values (Fig. S56). They also mentioned that they did not observe any Rb oxide molecules by mass spectrometry. This is inconsistent with the present calculations with higher partial pressures of O_2, in which significant Rb_2O(g) in the gas phase is expected (see P_{O_2} = 10^{-4} Pa and 10^{-1} Pa in Fig. S56). A possible reason for this is the strong dependence of the Rb_2O(g) partial pressure on the oxygen partial pressure. Our calculations are done at P_{O_2} = 10^{-4} Pa (as well as 10^{-1} Pa and 10^{-7} Pa in the present case); at lower oxygen partial pressures, which are likely the conditions under which Hellman *et al.*[76] operated their mass spectrometer, Rb(g) becomes the dominant gas species.

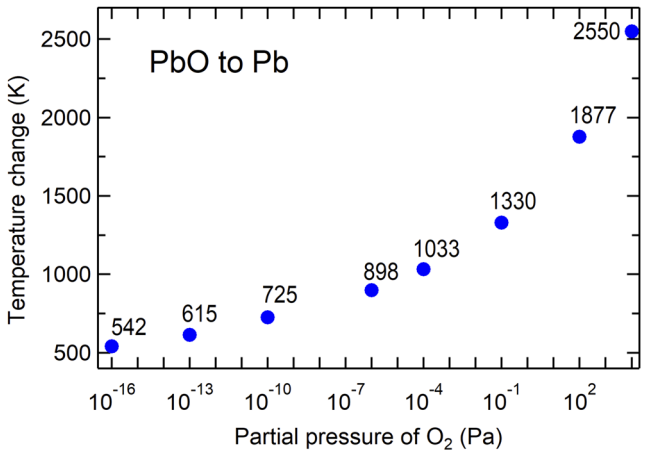


FIG. 3. Plot of the temperature (in K) at which the partial pressure of Pb(g) exceeds that of PbO(g) as a function of the partial pressure of O_2.

8. Re_2O_7(s, ℓ) (Fig. S57)

Through Knudsen cell studies, Skinner[77] found that Re_2O_7(s) evaporates congruently as Re_2O_7(g) at P_{O_2} = 2 × 10^{-4} Pa and T = 404 K. Due to a small amount of O_2 that simultaneously vaporized, some residual ReO_3(s) was left in the cell. The ions exhibiting the highest signal in Skinner's mass spectrometry study are in the following order: Re_2O_7, ReO_3, ReO_2, Re_2O_6, and Re_2O_5. In the present calculations (Fig. S57 as well as Table I), Re_2O_7 is the dominant gas species followed by Re_2O_6, which shares the stoichiometric ratio of ReO_3. To the best of our knowledge, Re_2O_7(s, ℓ) has not yet been used as an oxide source for MBE growth. Like B_2O_3, Re_2O_7 is very hygroscopic, which may limit its applications.[78]

9. As_2O_3(ℓ)(Fig. S5), Sb_2O_3(ℓ) (Fig. S60), and SnO(ℓ) (Fig. S65)

Figure S5 indicates liquid As_2O_3(ℓ) is a stable phase at higher temperatures (T > 677 K) transformed from solid As_2O_5(s). In the temperature range 677 K–1274 K, As_2O_3(ℓ) is a possible ideal MBE source with the dominant gas species of As_4O_6(g) at P_{O_2} = 10^{-4} Pa; see also Table I.

The behavior calculated for Sb_2O_3 is analogous to that of As_2O_3. At higher temperatures (T > 997 K), liquid Sb_2O_3(ℓ) is a stable phase transformed from solid SbO_2(s). Figure S60 as well as Table I shows that Sb_2O_3(ℓ) is also a possible ideal MBE source with the dominant gas species being Sb_4O_6(g) in the temperature range of 997 K–1429 K. Nearly congruent evaporation of Sb_2O_3(ℓ) is calculated to occur over the temperature range 997 K–1398 K at P_{O_2} = 10^{-4} Pa.

Similar to As_2O_3(ℓ) and Sb_2O_3(ℓ), at higher temperatures (T > 1498 K), liquid SnO(ℓ) becomes a stable phase. Figure S65 as well as Table I shows that SnO(ℓ) is also a possible ideal MBE source with the dominant gas species being Sn_1O_1(g) when T > 1498 K. SnO and SnO_2 are discussed further in Sec. III B 1.

Note that the solid phases of As_2O_3(s), Sb_2O_3(s), and SnO(s) are metastable, but they evaporate nearly congruently based on our calculations; see Figs. S5, S60, and S65 and Table III. Both As_2O_3(s) and Sb_2O_3(s) have been used as source materials in oxide MBE and were observed to evaporate congruently by Stall.[74] In his study, Stall noted the much lower vapor pressure of Sb_2O_3 (~10^{-2} Torr) compared with As_2O_3 (~10^{2} Torr) at 673 K.[74] To provide the desired flux of Sb_4O_6(g), the effusion cell containing Sb_2O_3(s) was operated at a temperature around 750 K, at which our calculations

© Author(s) 2020

indicate that SbO_2(s) is the stable phase. Nonetheless, Sb_2O_3(s) was observed to behave as an ideal MBE source by providing a molecular beam with the same stoichiometry as the source material [consistent with our calculation that the dominant species in the gas phase is Sb_4O_6(g)].

10. SeO_2(s, ℓ) (Fig. S62)

The calculated evaporation behavior of SeO_2(s) is shown in Fig. S62 as well as Table I. The results indicate that the gaseous SeO_2 species is dominant when SeO_2(s) is heated and agree well with Knudsen evaporation measurements between 360 K and 660 K.[22,79,80]

Metal oxides including SeO_2 as well as SnO_2, ZnO, TiO_2, VO, and WO_3 are particularly good gas sensors because the electrical conductivity of the thin film changes with gas adsorption.[81,82] Manno *et al.*[82] studied both SeO_2–SnO_2 and SeO_2–In_2O_3 thin films for applications in NO_x sensors. The SeO_2–In_2O_3 thin films were made by evaporating an InSe source and post-annealing the film in O_2. The SeO_2–SnO_2 thin films on the other hand were deposited onto an unheated quartz substrate by vaporizing 99.999% pure SeO_2 and SnO_2 with $P_{O_2} = 5 \times 10^{-5}$ Pa. After deposition, the films were annealed in flowing oxygen at 400 °C. The specific evaporation behavior of SeO_2 and SnO_2 is not discussed by the authors,[82] but it is likely that SnO_x species were in the vapor since SnO_x species from an SnO_2 source were noted under similar evaporation conditions.[11]

11. ThO_2(s) (Fig. S71) and PuO_2(s) (Fig. S55)

In agreement with the present calculations (Fig. S71 as well as Table I), the dominant gas species given off by a ThO_2 source in a Knudsen cell was shown to be ThO_2(g).[22] The evaporation behavior of ThO_2 is, however, not well studied in the literature, and the use of ThO_2 source materials in MBE is not reported. Similar to ThO_2(s), PuO_2(s) has not been reported as an MBE source either. In addition, no Knudsen cell evaporation studies could be found for PuO_2 in the literature.

12. Tl_2O(s, ℓ) (Fig. S73)

Tl_2O was calculated by Lamoreaux *et al.*[26] to exhibit congruent evaporation behavior under reducing conditions. Tl_2O is more stable than Tl_4O_3 and Tl_2O_3 at low oxygen partial pressures, which makes it ideal for the MBE vacuum environment.[26,83] Tl_2O powder is widely available from commercial distributors but is quite toxic. One concern with Tl_2O is its high reactivity with O_2 and many other elements at elevated temperatures.[83] Holstein[83] used an argon atmosphere to mitigate this issue and found the vapor pressure of Tl_2O(g) over the Tl_2O(s) source to be 29 Pa at 820 K, which agrees well with the evaporation behavior calculated in the present work (Fig. S73 and Table I). Tl_2O has been used in the growth of thin films of the high-temperature superconductors Tl–Ba–Ca–Cu–O and Tl–Pb–Sr–Ca–Cu–O, but no literature was found showing Tl_2O(s, ℓ) used as a source material in MBE.[83]

13. WO_3(s) (Fig. S77)

WO_3(s) is described to vaporize polymerically like MoO_3(s);[22] see Fig. S77 vs Fig. S41. A Knudsen cell evaporation study by Blackburn *et al.*[84] showed that $(WO_3)_3$ is the dominant vapor species. WO_2 is also a vapor species but is reported to decompose into $(WO_3)_3$ and W species.[84] The latter observation is not reflected in the present calculations (Fig. S77 and Table I), since the partial pressures of WO_2 and W in the present calculations are many orders of magnitude lower than that of W_3O_9 or any of the W_xO_{3x} species. The results shown in Fig. S77 are consistent with a heated charge of WO_3 that provides a beam of W_3O_9 as described in the Knudsen cell study of Blackburn *et al.*[84] Li *et al.*[85] used WO_3 powder as an MBE source to successfully grow WO_3 thin films for applications as a photocatalyst. In their experiments, WO_3 powder was evaporated from a high-temperature effusion cell and deposited as an epitaxial WO_3 film at a substrate temperature of 773 K in the presence of activated oxygen species from an oxygen plasma operating at $P_{O_2} = 4 \times 10^{-4}$ Pa.[85]

B. Stable solid oxide with incongruent evaporation

Having established which binary oxides evaporate nearly congruently, we next consider the possibility that a metastable binary oxide (if there were some way to produce it and constrain it from not decomposing in the solid state) would evaporate nearly congruently when heated. Table II summarizes the binary oxides that do not meet criterion 3 for nearly congruent evaporation (see Sec. II C) but evaporate incongruently instead. Such oxides are not ideal as the composition of the source will generally change over time as it becomes depleted in some component, but they might still be useful for MBE if they provide a desired gaseous species. In addition to considering the binary oxides in Table II, the species emanating from them with the highest partial pressure, i.e., the dominant gas species, were separately investigated as metastable sources to see if nearly congruent evaporation exists for those species. TcO_2 was also investigated but is omitted from the present work because it exhibits a decrease in vapor pressure with the increasing temperature in our calculations.

1. SnO_2 (Fig. S65)

Figure S65 shows the calculated evaporation behavior of SnO_2 as a function of temperature, where the gaseous species SnO is dominant above 1128 K in equilibrium with solid SnO_2 (see also Table II). To provide MBE-relevant fluxes, the temperature of the SnO_2 source is about 1350 K–1400 K, so when an SnO_2 source is used in oxide MBE, SnO is indeed the dominant species in the gas phase. SnO_2 was first used as a source in oxide MBE to achieve *n*-type doping of Ga_2O_3 with Sn^{4+}.[86] More recently, it has been used to grow $BaSnO_3$[10,11] and SnO.[87] The La-doped $BaSnO_3$ films grown by MBE with an SnO_2 source exhibit the highest mobility[10,11] and the best transistor performance[55] achieved to date, demonstrating SnO_2 as a viable MBE source.

Because SnO(g) is the dominant evaporating species, the use of SnO_2(s) as an MBE source also provides a possible route to grow Sn^{2+}-containing compounds such as *p*-type semiconductors that are predicted to have high mobility including SnO,[87,88] $K_2Sn_2O_3$,[87] $Rb_2Sn_2O_3$,[87] and Ta_2SnO_6.[88,89] Note that Sn^{2+} is a difficult oxidation state to stabilize. Many thermodynamic phase diagrams, e.g., those for Sn–O[90] as well as Sn–SnO_2,[91] omit SnO considering it to be metastable and to disproportionate into Sn and SnO_2; this agrees with the present thermodynamic analysis shown in Fig. S65. Being able to deliver a molecular beam of SnO to the substrate surface greatly simplifies the synthetic challenge to preparing

© Author(s) 2020

TABLE II. Incongruent evaporation of stable solid oxide sources under the following conditions: P_{O_2} = 10^{-4} Pa, fixed gas phase at zero amount, fixed T, and $n(M)$ = 1 mol.

Element	Solid oxide source	T-range (K)[a]	Dominant gas species	T-range (K)[b]
Si	SiO_2_cristobalite	700–1800	SiO	1570–1800
Sc	Sc_2O_3	700–2500	ScO_2, ScO	2170–2400, 2400–2500
V	V_2O_3	1289–1800	VO_2	1360–1800
Ga	Ga_2O_3	700–1800	Ga_2O	1362–1800
Ge	GeO_2	700–1389	GeO	1010–1800
As	As_2O_5	300–677	As_4O_6	612–1312
Rb	Rb_2O	517–778	Rb_2O, Rb	660–1800
Y	Y_2O_3	700–2500	YO_2	2000–2500
Zr	ZrO_2	700–2800	ZrO	2490–2800
In	In_2O_3	700–1676	In_2O	1218–1800
Sn	SnO_2	700–1498	SnO	1128–1800
Sb	SbO_2	700–997	Sb_4O_6	792–1429
Te	TeO_2	700–913	Te_2O_2	760–892
Cs	CsO_2	300–754	Cs_2O_2, Cs_2O	546–614, 614–700
La	La_2O_3	700–2500	LaO	1960–2500
Ce	Ce_2O_3	1988–2500	CeO	1940–2500
Pr	Pr_2O_3	1361–2500	PrO	1934–2500
Nd	Nd_2O_3	700–2500	NdO	1980–2500
Pm	Pm_2O_3	700–2593	PmO	2010–2926
Sm	Sm_2O_3	700–2500	SmO	2050–2460
Gd	Gd_2O_3	700–2500	GdO	2190–2500
Tb	Tb_2O_3	800–2500	TbO	2290–2500
Dy	Dy_2O_3	700–2500	DyO	2270–2500
Ho	Ho_2O_3	700–2500	HoO	2320–2500
Er	Er_2O_3	700–2500	ErO	2350–2500
Lu	Lu_2O_3	700–2500	LuO	2450–2500
Hf	HfO_2	700–3000	HfO, O	2640–3000
U	U_3O_8	525–939	U_2O_6	518–1800

[a]Temperature range where the oxide source is stable.
[b]Temperature range where the oxide gas species is dominant.

Sn^{2+}-containing materials. Furthermore, for the synthesis of anti-perovskites such as Sr_3SnO, it is preferable to have SnO arrive to the growth surface pre-oxidized and without any excess oxygen in order to avoid the undesired reaction of Sr_3SnO with excess oxygen to form unwanted SrO.[92] Finally, the present work (Fig. S65) also indicates that SnO(s) can be a metastable source that nearly congruently evaporates as SnO.

Following the recent experimental work of Hoffmann *et al.*,[39] we also examined the gas species for evaporation from a two-phase mixture of SnO_2(s) + Sn(ℓ) that has an overall composition SnO. Figure 4 shows that SnO(g) is the dominant gas species, indicating that a mixture of SnO_2(s) + Sn(ℓ) is also an ideal MBE source providing the nearly congruent evaporation of SnO; see a complete list of the two-phase mixtures examined in Table S2. As discussed in Sec. II A, the partial pressure of O_2 in the two-phase mixture is much lower than the typical MBE background value of 10^{-4} Pa, e.g., its value for a two-phase mixture of SnO_2(s) + Sn(ℓ) at 1200 K is about 10^{-9} Pa. The partial pressures of O_2 and all other species in the gas phase are determined by the two-phase equilibrium and are independent of the relative amounts of SnO_2(s) and Sn(ℓ) in the system. The use of equal amounts of SnO_2(s) and Sn(ℓ) to give the nominal SnO composition of the source may simplify experimental control if SnO_2(s) and Sn(ℓ) have similar evaporation rates. If the two condensed phases have very different evaporation kinetics, one may adjust the relative amounts of each phase in the two-phase mixture to provide the desired partial pressures in the MBE beam. Additional impacts of the metal-to-oxide ratio will be discussed in a forthcoming paper where the S-MBE method is more systematically examined.[93]

2. Ga_2O_3 (Fig. S27)

The present calculations (Fig. S27) show that Ga_2O_3(s) provides a beam of Ga_2O(g). This is in agreement with the experiments performed by Butt *et al.*[94] demonstrating that Ga_2O is the dominant gas species over Ga_2O_3(s). We did not investigate the nearly congruent evaporation of Ga_2O because Ga_2O(s) is not available in the SSUB5 database[27] [note that Ga_2O(s) is not a stable phase at 0 K according to first-principles calculations in the OQMD database].[95]

Ga_2O_3 thin films have several applications, including gas sensing. Its large bandgap, ability to be doped with n-type carriers,

© Author(s) 2020

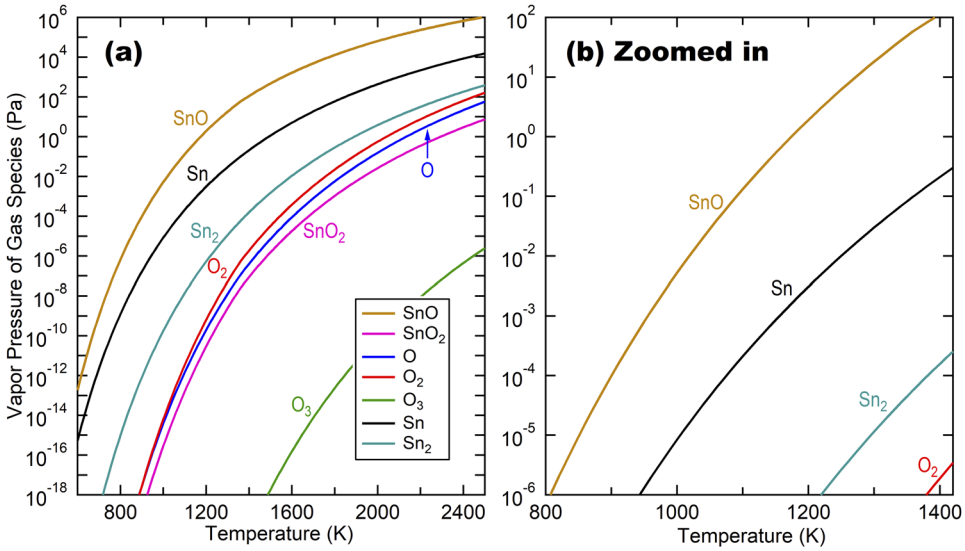


FIG. 4. (a) Calculated partial pressures of gas species for the evaporation of a two-phase mixture of SnO_2(s) + Sn(ℓ) with an overall composition of SnO and (b) a zoomed-in view in the pressure range of interest for oxide MBE. The conditions for the calculations are fixed gas phase at zero amount, n(Sn) = 1 mol, and $n(O_2)$ = 0.5 mol. Note that liquid Sn(ℓ) is stable at T > 505 K, solid SnO_2(s) is stable at T < 1359 K, and liquid SnO(ℓ) is stable at T > 1359 K. Hence, the phase regions are "Gas + SnO_2(s) + Sn(ℓ)" when T < 1359 and "Gas + SnO(ℓ)" when T > 1359 K in this figure, where the mole fraction of gas phase is fixed at zero amount.

relatively high mobility, and high Baliga figure of merit that is second only to diamond also attract tremendous interest for this semiconductor to be used for high-power electronics and ultraviolet (UV) detectors.[13,14] The growth of Ga_2O_3 thin films by MBE is a burgeoning area of research. Although most groups use Ga(ℓ) as the MBE source,[86,96–100] both amorphous[101] and epitaxial[102] films of Ga_2O_3(s) have been grown by MBE from a Ga_2O_3(s) source.

Another route to produce a molecular beam of Ga_2O(g) is to use a mixture of Ga(ℓ) and Ga_2O_3(s) instead of the incongruent evaporation of Ga_2O_3(s).[38,39] Such an approach has the advantage that a much lower temperature is needed to provide the same flux of Ga_2O(g) in the molecular beam from a Ga_2O_3(s) + Ga(ℓ) mixture compared to that from just Ga_2O_3(s), see Fig. S27 and Table S2 with the partial pressure of O_2 being 10^{-22} Pa at 1000 K. A prior MBE work used an iridium crucible to contain Ga_2O_3(s) because of the reactivity of Ga_2O_3 at high temperatures (in excess of 1900 K) needed to grow Ga_2O_3 films by MBE from a pure Ga_2O_3(s) source.[101,102] This temperature is considerably higher than that expected from Fig. S27 to yield a Ga_2O(g) partial pressure of 10^{-1} Pa (~1500 K is expected). Using a 5:1 mixture of Ga:Ga_2O_3 decreases the temperature of the crucible, i.e., the temperature needed to reach the same vapor pressure of Ga_2O(g), by about 500 °C.[38] A more recent MBE study shows similar temperature lowering for a 3.8:1 mixture of Ga:Ga_2O_3.[39] Exploiting molecular beams of suboxides such as Ga_2O(g) to grow films of compounds such as Ga_2O_3(s) is a powerful alternative to conventional MBE with many advantages; this approach is termed suboxide-MBE (S-MBE).[93]

3. TeO_2 (Fig. S70)

TeO_2 thin films have applications as gamma radiation detectors due to their sensitivity to gamma radiation. Sudha *et al.*[103] thermally evaporated TeO_2 powder onto a glass substrate at 10^{-3} Pa to form TeO_2 amorphous thin films for gas sensing; these amorphous films could be subsequently annealed to make them crystalline. The congruent evaporation behavior reported in Sudha *et al.*'s work[103] disagrees with the incongruent evaporation calculated in the present study of TeO_2(s) sublimation to Te_2O_2(s) at 760 K–892 K, although TeO_2(s) is the dominant gas species below 760 K (Fig. S70). Unfortunately, Sudha *et al.*[103] did not provide a temperature for the thermal evaporation of the TeO_2 powder to allow for comparison between their work and the present study. Additionally, Fig. S70 shows that the vapor pressures of Te_2O_2, TeO_2, and Te_2O_4 gas species decrease at temperatures above 913 K, while the vapor pressures of the other gas species continue to increase based on the present thermodynamic calculations.[27]

4. Rare-earth (RE) oxides

The present calculations (see the figures in the supplementary material) indicate that the majority of the rare-earth oxides share a similar evaporation behavior that is described below. The majority are most stable in sesquioxide form and provide molecular beams of stoichiometric *RE*O (*RE* = rare earth), making them incongruent evaporation sources for MBE. There are, however, a few exceptions where the gas-phase species with the highest partial pressure is *RE* or REO_2:

- **Supply *REO*:** Sc_2O_3, La_2O_3, Ce_2O_3 (and CeO_2), Pr_2O_3, Nd_2O_3, Pm_2O_3, Sm_2O_3, Gd_2O_3, Tb_2O_3, Dy_2O_3, Er_2O_3, and Lu_2O_3.
- **Supply *RE*:** Eu_2O_3 (and EuO), Tm_2O_3, and Yb_2O_3.
- **Supply REO_2**: Y_2O_3.

a. Lanthanides with 2+ valence (Fig. S24). EuO(s), SmO(s), and YbO(s) are known to be stable as RE^{2+} ions in addition to their sesquioxide forms. EuO(s) is calculated to produce a beam of Eu metal when heated as is its sesquioxide counterpart, Eu_2O_3(s); see Fig. S24. Unfortunately, thermodynamic calculations for SmO(s) and YbO(s) as oxide MBE sources could not be performed because they are not included in the SSUB5 database.[27] Experimentally, YbO thin films have been grown by MBE, although using separate beams of ytterbium and O_2 to deposit YbO.[104] The same is true for the

© Author(s) 2020

growth of EuO by MBE: from separate beams of europium and O_2.[105–107]

b. Rare-earth sesquioxides. Many of these rare-earth sesquioxides have been investigated as high-K gate dielectrics for use in metal–oxide–semiconductor field-effect transistors (MOSFETs) because of their high dielectric constant, large bandgap, and thermodynamic stability in contact with silicon.[108–112] To investigate these rare-earth sesquioxides as a replacement for SiO_2 in MOSFETs, researchers have used MBE to deposit Sc_2O_3, Y_2O_3, La_2O_3, Pr_2O_3, Nd_2O_3, Gd_2O_3, and Lu_2O_3 films on silicon from solid oxide sources of these same materials, i.e., from Sc_2O_3(s),[113] Y_2O_3(s),[114] La_2O_3(s),[108] Pr_6O_{11}(s),[115,116] Nd_2O_3(s),[117] Gd_2O_3(s),[108,114,118] to Lu_2O_3(s).[108]

The evaporation behavior of the majority of the sesquioxides proceeds as follows based on high-temperature Knudsen effusion mass spectrometry:[119]

$$RE_2O_3(s) = xREO(g) + (2-x)RE(g) + (3-x)O(g), \quad (2)$$

where $0 < x < 2$. The present calculations show that this evaporation behavior is exhibited by all rare-earth oxides except for Eu_2O_3 (and EuO), Tm_2O_3, Yb_2O_3, and Y_2O_3.

For Sc_2O_3 (Fig. S61), Y_2O_3 (Fig. S78), La_2O_3 (Fig. S36), Ce_2O_3 (Fig. S14), Pr_2O_3 (Fig. S53), Nd_2O_3 (Fig. S44), Pm_2O_3 (Fig. S52), Sm_2O_3 (Fig. S64), Gd_2O_3 (Fig. S28), Tb_2O_3 (Fig. S68), Dy_2O_3 (Fig. S21), Er_2O_3 (Fig. S22), and Lu_2O_3 (Fig. S38), our thermodynamic calculations indicate that all of these rare-earth sesquioxides should provide molecular beams of REO(g) when heated to a temperature where the dominant species in the gas phase has a vapor pressure of 10^{-1} Pa, i.e., the vapor pressure needed for typical oxide MBE growth. Unfortunately, the temperatures needed according to our vapor pressure calculations are near the limit of effusion cells for many of these RE_2O_3(s) sources, making it appropriate to use an e-beam evaporator or laser thermal evaporator to produce REO(g) molecular beams with source longevity.[120]

Stolyarova *et al.*[22,121] listed YO(g) as the dominant vapor constituent of thermally evaporated Y_2O_3(s). In the present calculations (Fig. S78), however, YO_2(g) is shown to be the dominant gas species when a Y_2O_3 source is heated in the temperature range of 1980 K < T < 2680 K, and YO(g) becomes the dominant vapor constituent when T > 2680 K. By omitting YO_2(g), YO(g) will be the dominant vapor constituent when T > 2370 K (Fig. S78). From the present study of the Y–O system, we note that calculations that disagree with experiments could be because certain gas species are added or omitted from the oxide systems in the SSUB5 database.[27] This is also seen in other systems such as the Pb–O system where the Pb_nO_n species are omitted from the SSUB5 database but included in the analysis by Lamoreaux *et al.*[26]; see Sec. III A 5.

For Eu_2O_3 (and EuO), the present calculations (Fig. S24) reveal that Eu_2O_3(s) and EuO(s) should evaporate as Eu(g), which offers no advantage in using oxide sources over elemental europium. The advantage of europium metal is that it can be melted into the crucible to provide a dense fill with good thermal contact to the crucible (and surrounding thermocouple). Elemental europium has been used in oxide MBE for the growth of $EuTiO_3$[122] and EuO.[105–107]

For Tm_2O_3, no literature on the evaporation behavior of Tm_2O_3 could be found to corroborate that Tm_2O_3 evaporates as a gas of the elemental metal thulium. If this is the case, a Tm_2O_3 source would offer no advantage over using elemental thulium metal as an MBE source (see Fig. S74).

Following a recent publication by Hoffmann *et al.*,[39] we also examined the gas species as a function of temperature for a two-phase mixture of RE_2O_3 + RE that has an overall composition of REO. It is shown that the dominant gas species is in general RE(g) and the second dominant gas species is REO(g); see Table S2 and associated figures, including those for the two-phase mixture case with cerium (Fig. S14), dysprosium (Fig. S21), erbium (Fig. S22), europium (Fig. S24), gadolinium (Fig. S28), holmium (Fig. S32), lanthanum (Fig. S36), lutetium (Fig. S38), neodymium (Fig. S44), promethium (Fig. S52), praseodymium (Fig. S53), samarium (Fig. S64), terbium (Fig. S68), thulium (Fig. S74), and ytterbium (Fig. S79). At high temperatures, REO(g) is calculated to be the most dominant gas species, for example, T > 1136 K for CeO(g), T > 1308 K for LaO(g), and T > 2239 K for PrO(g). For other RE elements, however, the temperatures are extremely high (≫3000 K) in order to make the dominant gas species REO(g).

C. Metastable solid oxide with nearly congruent evaporation

Table III summarizes the metastable oxides that evaporate nearly congruently based on the present calculations. Of these, the oxides IrO_2, PtO_2, and RuO_2 would give the most advantage because their stable counterparts are elemental metals (iridium, platinum, and ruthenium) meaning no other solid (or liquid) binary oxide sources are available to create molecular beams of these oxides. Similar to Table I, Table III also lists the temperature range for nearly congruent evaporation defined by $|\Delta x(O_2)| < 0.01$; see Eq. (1).

The concern with using metastable oxides as source materials for MBE is that these compounds could decompose into more stable compounds and in the process pollute the MBE vacuum with O_2 species. For metastable oxides, there are two scenarios that can occur when the oxide is heated, which depend on the kinetics of the compound as discussed in Sec. II A. The kinetics of oxide decomposition is beyond the scope of the present work, but a literature search has been conducted for experimental evidence of the successful use of metastable oxides in MBE; the details are described below. Furthermore, the decomposition of RuO_2 has been studied in the present work by differential thermal analysis with simultaneous thermogravimetry (DTA/TG) to follow the decomposition process under conditions approaching those in the high-vacuum MBE environment.

1. Cs_2O (Fig. S19)

Figure S19 shows that Cs_2O(s) is a metastable phase, but it evaporates nearly congruently in the temperature range of 705 K–1059 K due to the value of $|\Delta x(O_2)| < 0.01$ [see Eq. (1)]; see Table III.

2. SiO (Fig. S63) and GeO (Fig. S29)

From Table II, it can be seen that the evaporation of SiO_2 and GeO_2 is incongruent and provides molecular beams of SiO and GeO,

© Author(s) 2020

TABLE III. Metastable sources under the following conditions: $P_{O_2} = 10^{-4}$, fixed gas phase at zero amount, fixed T, and $n(M) = 1$ mol, which evaporate nearly congruently.

Element	Solid oxide source	Dominant gas species	Stable oxide[a]	T-range[b]	T-range[c]
As	As_2O_3	As_4O_6	As_2O_5	611–677[d]	650–1278
Cs	Cs_2O	Cs_2O	CsO_2	612–1476	705–1059
Ge	GeO	GeO	GeO_2	>1290	>1595
Ir	IrO_2	IrO_2	Ir	1260–1520	1390–1425
Nb	NbO_2	NbO_2	$Nb_2O_5(\ell)$	1550–2590	1768–2283
Os	OsO_4	OsO_4	OsO_2	200–1000	200–1000
Pt	PtO_2	PtO_2	Pt	846–1253	915–1156
Re	ReO_3[e]	Re_2O_6	Re_2O_7	>848	>around 850
Ru	RuO_2	RuO_2	Ru	1220–1480	1326–1368
Sb	Sb_2O_3	Sb_2O_3	SbO_2	>528	555–1391
Si	SiO	SiO	SiO_2	>1320	1556–2983
Sn	SnO	SnO	SnO_2	>889	983–1750
Ti	TiO_2 anatase	TiO_2	$Ti_4O_7(\ell)$	1790–2220	1914–2007
Ti	TiO_2 rutile	TiO_2	$Ti_4O_7(\ell)$	1800–2220	1952–2025
U	UO_3	U_2O_6	U_3O_8	>517	544–1900
V	V_2O_5	V_4O_{10}	V_2O_4	804–2116	838–2092

[a]Stable oxide phase under given conditions.
[b]Temperature range (in K) where the oxide gas species is dominant.
[c]Temperature range (in K) of nearly congruent evaporation as defined by Eq. (1) for an absolute value of $\Delta x(O_2) < 0.01$.
[d]Liquid As_2O_3 is stable at $T > 677$ K and is an ideal MBE source (see Table I).
[e]Thermodynamic calculations of ReO_3(s) were performed at $P_{O_2} = 10^{-15}$ Pa where its gas phase is metastable, a requirement for our calculations under the constraint that the fixed gas phase has zero amount. This zero amount requirement is not satisfied for ReO_3(s) at $P_{O_2} = 10^{-4}$ Pa.

respectively. Unfortunately, these latter monoxides are not in the SSUB5 database.[27] Amorphous SiO(am) is well-known to evaporate nearly congruently;[22–24] its thermodynamic properties[30] were added to the database in the present work. In addition, the enthalpy of formation of the amorphous GeO(am)[29] was also added. The fact that SiO(am) evaporates nearly congruently makes it of interest for synthesizing Si^{2+}-based compounds in MBE, and GeO(am) behaves similarly to SiO(am) and could be a route to Ge^{2+}-based compounds.

Figure S63 illustrates the evaporation behavior of SiO(am) calculated at $P_{O_2} = 10^{-4}$ Pa, showing that SiO(am) gives off SiO_2(g) species at low temperatures (below 1320 K) and SiO(g) species at higher temperatures (above 1320 K). Stoichiometric SiO has been found to evaporate from an SiO(am) source at temperatures in the vicinity of 1520 K in high vacuum (~10^{-6} Pa),[23,24] which is consistent with the results shown in Fig. S63. When the evaporation behavior of SiO(am) is calculated under a stronger vacuum such as $P_{O_2} = 10^{-15}$ Pa, the SiO gas species becomes dominant at lower temperatures (above 990 K) than it does in lower vacuum (e.g., 1320 K as mentioned above). Stolyarova and Semenov[22] indicated that SiO(am) evaporates congruently in a Knudsen cell experiment between 1175 K and 1410 K. This is confirmed by the present calculations. Should an interesting Si-containing multicomponent oxide warrant investigation, SiO(am) could be used to provide a molecular beam of SiO(g). One system that might be relevant is the growth of Si-doped Ga_2O_3, where the high oxidant pressures involved in the growth of Ga_2O_3 result in the oxidation of the surface of the traditional Si(s) doping sources used in MBE.[34] This oxidation results in the flux emanating from a Si(s) source to change rapidly over time, impeding the use of silicon as a dopant in the growth of oxides by MBE.

The calculated evaporation from a two-phase mixture of SiO_2 + Si with an overall composition SiO (Fig. S63) indicates that SiO(g) is the dominant gas species in the temperature range of study (see also Table S2) in agreement with a recent report.[39] Similar to the Si–O case, GeO_2(s) is the stable phase up to 872 K, beyond which GeO(am) becomes stable based on the SSUB5 database and the enthalpy of formation of GeO(am) from the literature;[29] see also the note in the figure caption of Fig. S29. GeO(g) is the dominant gas species when the solid/liquid source is GeO_2(s), GeO(am), or a two-phase mixture of GeO_2 + Ge (see also Table S2). Our conclusions for the GeO_2 + Ge mixture are in good agreement with the thermodynamic calculations by Hoffmann *et al.*[39]

3. IrO_2, PtO_2, and RuO_2 (Figs. S34, S54, and S59)

IrO_2(s) and RuO_2(s) are of particular interest for oxide MBE because in elemental form, Ir(s) and Ru(s) sources have such low vapor pressures that today's MBE effusion cells are unable to evaporate them. Solid iridium and ruthenium can be evaporated by electron-beam evaporation sources, but the stability of the flux from an electron-beam evaporator is inferior to the flux stability provided by effusion cells. IrO_2 and RuO_2 are components of materials with a multitude of interesting properties and electronic structures due to the high spin–orbit coupling and electron correlations present in materials containing these constituents. Examples

© Author(s) 2020

include the unconventional superconductor Sr_2RuO_4,[123] the itinerant metamagnet $Sr_3Ru_2O_7$,[124] features in the electronic structure of doped Sr_2IrO_4 that are akin to the cuprate high-temperature superconductors,[125] the magnetically ordered Mott insulator Na_2IrO_3,[126] Weyl semimetals in the $RE_2Ir_2O_7$ pyrochlores,[127] and heterostructures containing these materials that could, for example, host a two-dimensional gas of magnetic monopoles.[128] MBE sources that provided stable fluxes of IrO_2 and RuO_2 could thus greatly enhance the ability of oxide MBE to create iridates and ruthenates that are customized with atomic-layer precision.

IrO_2 and RuO_2 are commercially available powders, so it is important to investigate these oxides even though they are metastable under MBE deposition conditions. In the present calculations, metastable IrO_2 and RuO_2 are found to evaporate nearly congruently as shown in Figs. S34 and S59, respectively. IrO_2 and RuO_2 thin films have been fabricated using MBE; however, they were made using elemental iridium or ruthenium sources heated by an electron-beam evaporator with oxidation provided by a separate molecular beam of ozone.[129,130] No literature was found on the evaporation of RuO_2 or the use of RuO_2 as a source in oxide MBE.

The suitability of IrO_2 and RuO_2 to create molecular beams depends on the kinetics of their decomposition as discussed in Sec. II A. For example, IrO_2 could follow two scenarios when heated in the MBE crucible,

$$IrO_2(s) \rightarrow Ir(s) + O_2(g), \tag{3}$$

$$IrO_2(s) \rightarrow IrO_2(g). \tag{4}$$

The first scenario, Eq. (3), shows $IrO_2(s)$ decomposition into Ir(s) and $O_2(g)$, which would pollute the MBE chamber with oxygen species. The Ir(s) species would then evaporate with the partial pressures of the gas species shown in Fig. S34. If this first pathway is relevant, $IrO_2(s)$ as an MBE source offers no advantages (and many disadvantages) over an elemental Ir(s) source. In the second scenario, Eq. (4), as $IrO_2(s)$ is heated up, it evaporates $IrO_2(g)$ as shown in Fig. S34. These $IrO_2(g)$ species would be emitted as a molecular beam, which would travel to the substrate in the MBE chamber. In this latter case, the $IrO_2(g)$ species would be depleted at the surface of the $IrO_2(s)$ source as it evaporates. To restore equilibrium, the IrO_2 species would produce more $IrO_2(g)$. In this second scenario, the $IrO_2(s)$ species evaporates into $IrO_2(g)$ much faster than it decomposes; for oxide MBE, this would be the preferred kinetic pathway to make $IrO_2(s)$ a viable MBE source material. Another thing to consider is the energy required to break $IrO_2(s)$ into Ir(s) and $O_2(g)$. If the activation barrier is high, it would be much more likely for $IrO_2(s)$ to evaporate as IrO_2, where only intermolecular bonds have to be broken. In addition to metastable IrO_2 and RuO_2, the present calculations (Fig. S54 and Table III) also indicate that metastable PtO_2 evaporates nearly congruently in the temperature range of 915 K–1156 K at $P_{O_2} = 10^{-4}$ Pa.

As IrO_2, PtO_2, and RuO_2 share the chemical similarity of all being 4+ oxides of platinoids, we performed some preliminary experiments on one of these compounds, $RuO_2(s)$, and found that it decomposes before it evaporates. Specifically, our experiments indicate that when heated, $RuO_2(s)$ undergoes the reaction $2RuO_2(s) \rightarrow Ru_2O_3(s) + \frac{1}{2}\ O_2(g)$. The predominant species that $RuO_2(s)$ gives off when heated is thus $O_2(g)$, making it not useful as an MBE source. Figure 5 shows two thermogravimetric (TG) measurements where $RuO_2(s)$ was heated under ambient pressure in an Ar/O_2 mixture or in nominally pure Ar with 99.9999%–99.999% purity, which results in the stated oxygen partial pressures.[131] Between room temperature and 773 K, the changes in the first TG step occur, corresponding to $\Delta m/m = -5.7\%$ (oxidizing atmosphere) or −6.0% (Ar). These observed mass changes would be consistent with the reaction $2RuO_2(s) \rightarrow Ru_2O_3(s) + \frac{1}{2}\ O_2(g)$, where $\Delta m/m$ of the condensed phases would be −6.0%. The decomposition of the remainder becomes significant above 1273 K–1370 K. Since $Ru_2O_3(s)$ is not in the SSUB5 thermodynamic database, this reaction is not predicted by our thermodynamic calculations. Nonetheless, Ru^{3+} is reported in halides, such as RuF_3 and $RuCl_3$, as well as in the oxide $LaRuO_3$.[132]

4. NbO_2 (Fig. S43)

NbO_2 has been shown to have NbO_2 species in the gas phase when evaporated from a Knudsen cell at 2050 K.[22] Having NbO_2 as the dominant species in the gas phase is expected regardless of whether evaporation occurs from metastable $NbO_2(s)$ or from the stable phase, $Nb_2O_5(\ell)$, at 2050 K. The present work (Fig. S43 and Table III) predicts that (metastable) NbO_2 evaporates nearly congruently between 1768 K and 2283 K at $P_{O_2} = 10^{-4}$ Pa. NbO_2 has useful metal-to-insulator transition electronic properties motivating its growth by MBE.[133] $NbO_2(s)$ could be a viable source for the growth of NbO_2 thin films and is worth trying as an MBE source.

5. ReO_3 (Fig. S57)

$ReO_3(s)$ is a metastable phase in the Re–O system, and it is expected that it could evaporate nearly congruently. In our thermodynamic calculations using $P_{O_2} = 10^{-4}$ Pa, however, the gas phase does not satisfy the requirement of having zero amount. So we performed ancillary thermodynamic calculations of $ReO_3(s)$ at a very

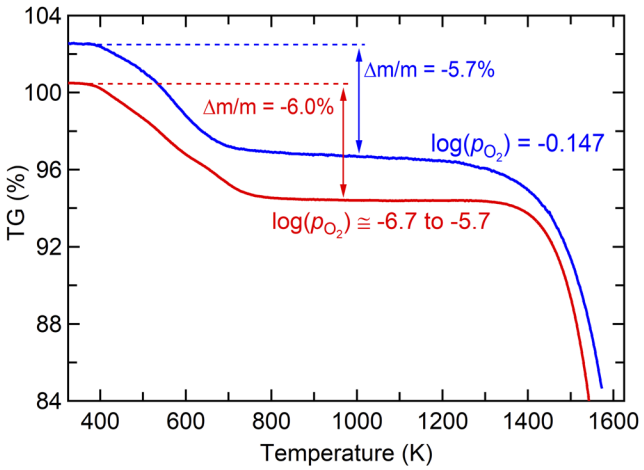


FIG. 5. Thermogravimetric (TG) curves of $RuO_2(s)$ heated in 71% O_2 + 29% Ar (blue curve) or in "pure" Ar (red curve). Here, P_{O_2} indicates the oxygen partial pressure in atm and $\Delta m/m$ shows the mass change in the TG curves.

© Author(s) 2020

TABLE IV. Metastable oxide sources under the following conditions: $P_{O_2} = 10^{-4}$, fixed gas phase at zero amount, fixed T, and $n(M) = 1$ mol, which evaporate incongruently.

Element	Solid oxide source	Dominant gas species	Stable oxide[a]	T-range (K)[b]
Cs	Cs_2O_2	Cs_2O	CsO_2	612–1030
Cs	Cs_2O_3	Cs_2O	CsO_2	612–880
Ce	CeO_2	CeO	Ce_2O_3	1880–2990
Pr	PrO_2	Pr_2O	Pr_2O_3	1600–2900
Pr	Pr_7O_{12}	Pr_3O	Pr_2O_3	1880–3000
Pr	Pr_6O_{11}	Pr_4O	Pr_2O_3	1650–2920
Tb	TbO_2	TbO	Tb_2O_3	1790–2500
Ta	Ta_2O_5	TaO_2	Ta_2O_5 liquid	2020–2740
Pb	Pb_2O_3	PbO	PbO yellow	700–1034
Pb	Pb_3O_4	PbO_2	PbO yellow	700–1034
Pb	PbO_2	PbO	PbO yellow	700–950

[a]Stable oxide phase under given conditions.
[b]Temperature range where the oxide gas species is dominant.

low oxygen partial pressure of $P_{O_2} = 10^{-15}$ Pa. The results of these calculations, shown in Fig. S57, indicate that ReO_3(s) is a metastable oxide that evaporates nearly congruently at $P_{O_2} = 10^{-15}$ Pa, i.e., the dominant gas species is Re_2O_6 when $T > 848$ K; see also Table III. It is expected that ReO_3(s) could be a viable source for the growth of ReO_3 thin films albeit our calculations were performed at $P_{O_2} = 10^{-15}$ Pa. ReO_3 is also discussed in Sec. III A 8.

6. TiO_2 (Fig. S72)

TiO_2 has been shown to evolve TiO species when evaporated from a Knudsen cell at 1920 K.[22] This result is unexpected from our thermodynamic calculations. If the initial TiO_2 loaded into the Knudsen cell decomposes into the stable phase, on heating to 1920 K, it would be Ti_4O_7(s) and the dominant species evaporated at 1920 K would be TiO_2(g). On the other hand, if TiO_2 loaded into the Knudsen cell remained in the metastable rutile polymorph at 1920 K, then the dominant species evaporated at 1920 K would also be TiO_2(g). Our calculations only show TiO to be the dominant vapor species at temperatures above 2220 K for both anatase and rutile TiO_2, which are both metastable at this temperature, at the 10^{-4} Pa O_2 partial pressure of the present work; see Fig. S72 as well as Table III.

7. UO_3 (Fig. S75)

Solid UO_3(s) is a stable phase when $T < 525$ K; at higher temperatures, the solid U_3O_8(s) becomes stable (>525 K). Figure S75 shows that U_2O_6(g) is the dominant gas species at temperatures $T > 517$ K and $P_{O_2} = 10^{-4}$ Pa [O_2(g) is dominant at $T < 517$ K]. Although U_2O_6(g) is the dominant species in the gas phase, the value of $|\Delta x(O_2)| > 0.01$ [see Eq. (1)] in the temperature range of 517 K–525 K due to the nonnegligible concentration of other species in the gas phase. This disqualifies UO_3(s) as an ideal MBE source from the definition of nearly congruent evaporation that we have used. It is worth mentioning that at an extremely low partial pressure of O_2(g), such as $P_{O_2} = 10^{-15}$ Pa, it is possible to make $|\Delta x(O_2)| < 0.01$ for UO_3(s).

As a metastable phase, the present calculations show that UO_3(s) evaporates nearly congruently in the temperature range of 544 K–1900 K at $P_{O_2} = 10^{-4}$ Pa; see Table III.

D. Metastable solid oxide with incongruent evaporation

Table IV shows the metastable oxide sources that exhibit incongruent evaporation. Based on the dominant species in the molecular beams from the stable sources that exhibit incongruent evaporation, these metastable oxides are calculated in the present work to see if they would exhibit nearly congruent evaporation. Unfortunately, they all exhibit incongruent evaporation as can be seen in the calculated figures in the supplementary material. Specifically, see Fig. S14 for the binary oxides containing cerium, Fig. S19 for those containing cesium, Fig. S50 for those containing lead, Fig. S53 for those containing praseodymium, Fig. S67 for those containing tantalum, and Fig. S68 for those containing terbium. These metastable incongruent evaporants offer no advantage over their stable incongruent evaporant counterparts and hence are not discussed further.

IV. SUMMARY

A comprehensive thermodynamic investigation regarding the evaporation behavior of 128 binary oxides has been performed to evaluate their suitability as MBE source materials. Based mainly on the SSUB5 database used in the present work,[27] we conclude that 16 solid or liquid oxides are most ideal for MBE, i.e., As_2O_3, B_2O_3, BaO, MoO_3, OsO_4, P_2O_5, PbO, PuO_2, Rb_2O, Re_2O_7, Sb_2O_3, SeO_2, SnO, ThO_2, Tl_2O, and WO_3. Of these, As_2O_3, B_2O_3, BaO, MoO_3, PbO, Sb_2O_3, and WO_3 have been utilized to date as MBE source materials. The remaining nine oxides await verification as good oxide source materials in MBE. The use of PbO(s) as a source material may be limited by the allowable O_2 partial pressure in the MBE chamber. Of the solid oxide sources that show incongruent evaporation, SnO_2 has been shown to work experimentally and produces

© Author(s) 2020

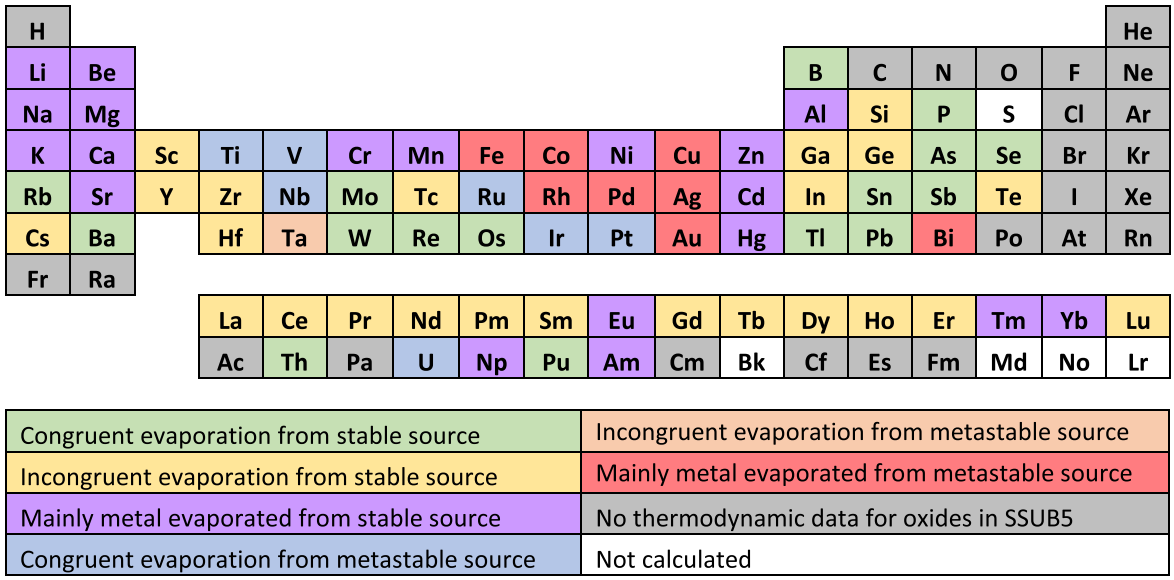


FIG. 6. Periodic table summarizing the evaporation behavior of binary oxides. Note that congruent evaporation is indicated whenever at least one of the oxides of a particular element evaporates nearly congruently (as defined in the text).

a molecular beam of mainly SnO(g). Although they do not meet the third criterion to be ideal MBE sources (i.e., nearly congruent evaporation; see Sec. II C), some oxides that meet the first criterion (i.e., solid or liquid metal-oxide source that is stable under the given conditions; see Sec. II C) may also work as oxide MBE source materials, like SnO_2 does. The amorphous and metastable phase SiO(s) is known to evaporate before it decomposes, making it suitable as an MBE source. The same may be true for other metastable phases including amorphous GeO(s) and SnO(s). Finally, a likely route to achieve the desired nearly congruent evaporation characteristic of an ideal MBE source—a characteristic that keeps the fluxes of the species in the molecular beams constant, because the composition of the source itself is not changing over the life of the source—is to use a two-phase mixture. Potential MBE sources of this mixture type are, for example, (Al_2O_3 + Al) to produce a molecular beam of Al_2O(g), (Ce_2O_3 + Ce) to produce CeO(g), (Ga_2O_3 + Ga) to produce Ga_2O(g), (GeO_2 + Ge) to produce GeO(g), (HfO_2 + Hf) to produce HfO(g), (In_2O_3 + In) to produce In_2O(g), (La_2O_3 + La) to produce LaO(g), (Pr_2O_3 + Pr) to produce PrO(g), (SiO_2 + Si) to produce SiO(g), (SnO_2 + Sn) to produce SnO(g), (Ta_2O_5 + Ta) to produce TaO_2(g), and (ZrO_2 + Zr) to produce ZrO(g); see the 27 cases examined in Table S2. Our conclusions for two-phase mixtures are in agreement with the recent thermodynamic calculations by Hoffmann *et al.*[39] for Al_2O(g), Ga_2O(g), GeO(g), In_2O(g), LaO(g), PrO(g), SiO(g), and SnO(g). Our predictions also identify four additional two-phase sources of interest for producing molecular beams of CeO(g), HfO(g), TaO_2(g), and ZrO(g).

Several trends are evident in the evaporation behavior of binary metal oxides. These are shown in Fig. 6. Alkali-metal oxides, alkaline-earth metal oxides, and some of the transition-metal oxides evaporate mainly elemental metal gas species and thus are not ideal for MBE. The rare-earth oxides and some of the transition metals surrounding them as well as the metalloid oxides exhibit incongruent evaporation. Oxides ideal for MBE are the column IVA oxides SiO, GeO, SnO, and PbO, although the first three of these are metastable (amorphous). In addition, there are disruptions to certain trends such as the evaporation of elemental metals from EuO, Tm_2O_3, and Yb_2O_3, which do not follow the incongruent evaporation trend of the other rare earths.

SUPPLEMENTARY MATERIAL

See the supplementary material for an alphabetical list of 128 solid and liquid oxides together with a list of 17 elements of which the most stable phase is not an oxide (Table S1), a list of 27 two-phase mixtures of a solid (or liquid) of pure element *M* in combination with one of its binary oxides yielding an overall composition of M_xO_y (Table S2), three illustrative examples of macro files to perform some of the Thermo-Calc calculations presented (Table S3), and an alphabetical list of supplemental figures (Figs. S1–S81) showing the calculated partial pressures of gas species over the phase(s) of interest.

ACKNOWLEDGMENTS

We acknowledge financial support from the National Science Foundation (NSF) through Grant No. CMMI-1825538 and the Platform for the Accelerated Realization, Analysis and Discovery of Interface Materials (PARADIM) under Cooperative Agreement No. DMR-1539918. B.J.B. was supported by a NASA Space Technology Research Fellowship (Grant No. 80NSSC18K1168). This material is based on the work supported by the Air Force Office of Scientific Research under Award No. FA9550-18-1-0529. D.G.S.

© Author(s) 2020

acknowledges stimulating interactions with O. Bierwagen, W. Braun, M. Budde, G. Christiani, R. Droopad, G. Hoffmann, J. P. Maria, and P. Vogt regarding oxide MBE utilizing oxide sources.

DATA AVAILABILITY

The data that support the findings of this study are available from the corresponding author upon reasonable request.

REFERENCES

[1] V. J. Folen, G. T. Rado, and E. W. Stalder, Phys. Rev. Lett. **6**, 607 (1961).
[2] I. Vrejoiu, G. Le Rhun, L. Pintilie, D. Hesse, M. Alexe, and U. Gösele, Adv. Mater. **18**, 1657 (2006).
[3] G. H. Jonker and J. H. Van Santen, Physica **16**, 337 (1950).
[4] A. J. Hauser, R. E. A. Williams, R. A. Ricciardo, A. Genc, M. Dixit, J. M. Lucy, P. M. Woodward, H. L. Fraser, and F. Yang, Phys. Rev. B **83**, 014407 (2011).
[5] H. P. J. Wijn, Nature **170**, 707 (1952).
[6] S.-E. Park and T. R. Shrout, J. Appl. Phys. **82**, 1804 (1997).
[7] J. Wang, Science **299**, 1719 (2003).
[8] A. Schilling, M. Cantoni, J. D. Guo, and H. R. Ott, Nature **363**, 56 (1993).
[9] T. Penney, M. W. Shafer, and J. B. Torrance, Phys. Rev. B **5**, 3669 (1972).
[10] S. Raghavan, T. Schumann, H. Kim, J. Y. Zhang, T. A. Cain, and S. Stemmer, APL Mater. **4**, 016106 (2016).
[11] H. Paik, Z. Chen, E. Lochocki, A. Seidner H., A. Verma, N. Tanen, J. Park, M. Uchida, S. Shang, B.-C. Zhou, M. Brützam, R. Uecker, Z.-K. Liu, D. Jena, K. M. Shen, D. A. Muller, and D. G. Schlom, APL Mater. **5**, 116107 (2017).
[12] E. Sachet, C. T. Shelton, J. S. Harris, B. E. Gaddy, D. L. Irving, S. Curtarolo, B. F. Donovan, P. E. Hopkins, P. A. Sharma, A. L. Sharma, J. Ihlefeld, S. Franzen, and J.-P. Maria, Nat. Mater. **14**, 414 (2015).
[13] M. Higashiwaki, K. Sasaki, H. Murakami, Y. Kumagai, A. Koukitu, A. Kuramata, T. Masui, and S. Yamakoshi, Semicond. Sci. Technol. **31**, 034001 (2016).
[14] M. Higashiwaki and G. H. Jessen, Appl. Phys. Lett. **112**, 060401 (2018).
[15] M. A. Herman and H. Sitter, *Beam Epitaxy: Fundamentals and Current Status*, 2nd ed. (Springer-Verlag, Berlin, 1996).
[16] D. G. Schlom, APL Mater. **3**, 062403 (2015).
[17] H. P. Nair, J. P. Ruf, N. J. Schreiber, L. Miao, M. L. Grandon, D. J. Baek, B. H. Goodge, J. P. C. Ruff, L. F. Kourkoutis, K. M. Shen, and D. G. Schlom, APL Mater. **6**, 101108 (2018).
[18] J. L. MacManus-Driscoll, M. P. Wells, C. Yun, J.-W. Lee, C.-B. Eom, and D. G. Schlom, APL Mater. **8**, 040904 (2020).
[19] H. P. Nair, Y. Liu, J. P. Ruf, N. J. Schreiber, S.-L. Shang, D. J. Baek, B. H. Goodge, L. F. Kourkoutis, Z.-K. Liu, K. M. Shen, and D. G. Schlom, APL Mater. **6**, 046101 (2018).
[20] H. Li, X. Hu, Y. Wei, Z. Yu, X. Zhang, R. Droopad, A. A. Demkov, J. Edwards, K. Moore, W. Ooms, J. Kulik, and P. Fejes, J. Appl. Phys. **93**, 4521 (2003).
[21] P. Moetakef, T. A. Cain, D. G. Ouellette, J. Y. Zhang, D. O. Klenov, A. Janotti, C. G. Van de Walle, S. Rajan, S. J. Allen, and S. Stemmer, Appl. Phys. Lett. **99**, 232116 (2011).
[22] V. L. Stolyarova and G. A. Semenov, *Mass Spectrometric Study of the Vaporization of Oxide Systems*, 2nd ed. (John Wiley & Sons, West Sussex, England, 1994).
[23] G. HASS, J. Am. Ceram. Soc. **33**, 353 (1950).
[24] M. Fernández-Perea, M. Vidal-Dasilva, J. I. Larruquert, J. A. Aznárez, J. A. Méndez, E. Gullikson, A. Aquila, and R. Soufli, J. Appl. Phys. **105**, 113505 (2009).
[25] R. H. Lamoreaux and D. L. Hildenbrand, J. Phys. Chem. Ref. Data **13**, 151 (1984).
[26] R. H. Lamoreaux, D. L. Hildenbrand, and L. Brewer, J. Phys. Chem. Ref. Data **16**, 419 (1987).
[27] Scientific Group Thermodata Europe (SGTE), in *Landolt-Boernstein New Ser. Gr. IV*, edited by Lehrstuhl fuer Theoretische Huettenkunde (Springer, Verlag Berlin Heidelberg, 1999).
[28] J.-O. Andersson, T. Helander, L. Höglund, P. Shi, and B. Sundman, Calphad **26**, 273 (2002).
[29] J. Drowart, F. Degrève, G. Verhaegen, and R. Colin, Trans. Faraday Soc. **61**, 1072 (1965).
[30] O. Kubaschewski and C. B. Alcock, *Metallurgical Thermochemistry*, 5th ed. (Pergamon, Elmsford, NY, 1979).
[31] F. Tesfaye, D. Sukhomlinov, D. Lindberg, P. Taskinen, and G. Akdogan, J. Chem. Thermodyn. **106**, 47 (2017).
[32] H. Lüth, *Solid Surfaces, Interfaces and Thin Films*, 6th ed. (Springer-Verlag, Berlin, 2015).
[33] S. Franchi, in *Molecular Beam Epitaxy*, edited by M. Henini (Elsevier, Amsterdam, 2013), pp. 1–46.
[34] N. K. Kalarickal, Z. Xia, J. McGlone, S. Krishnamoorthy, W. Moore, M. Brenner, A. R. Arehart, S. A. Ringel, and S. Rajan, Appl. Phys. Lett. **115**, 152106 (2019).
[35] Y. S. Kim, N. Bansal, C. Chaparro, H. Gross, and S. Oh, J. Vac. Sci. Technol., A **28**, 271 (2010).
[36] Y.-S. Kim, N. Bansal, and S. Oh, J. Vac. Sci. Technol., A **29**, 041505 (2011).
[37] Z. K. Liu and Y. Wang, *Computational Thermodynamics of Materials* (Cambridge University Press, Cambridge, UK, 2016).
[38] C. J. Frosch and C. D. Thurmond, J. Phys. Chem. **66**, 877 (1962).
[39] G. Hoffmann, M. Budde, P. Mazzolini, and O. Bierwagen, APL Mater. **8**, 031110 (2020).
[40] H. Aizaki and T. Tatsumi, in *Extended Abstracts of the 17th Conference on Solid State Devices and Materials* (The Japan Society of Applied Physics, Tokyo, 1985), p. 297.
[41] R. M. Ostrom and F. G. Allen, Appl. Phys. Lett. **48**, 221 (1986).
[42] M. Putkonen and L. Niinistö, Thin Solid Films **514**, 145 (2006).
[43] K. A. Stewart, V. Goulioukk, D. A. Keszler, and J. F. Wager, Solid-State Electron. **137**, 80 (2017).
[44] O. M. Moon, B.-C. Kang, S.-B. Lee, and J.-H. Boo, Thin Solid Films **464-465**, 164 (2004).
[45] A. Edukondalu, S. Rahman, S. K. Ahmmad, A. Gupta, and K. Siva Kumar, J. Taibah Univ. Sci. **10**, 363 (2016).
[46] A. I. Kingon, S. K. Streiffer, C. Basceri, and S. R. Summerfelt, MRS Bull. **21**, 46 (1996).
[47] C. J. G. Meyers, C. R. Freeze, S. Stemmer, and R. A. York, Appl. Phys. Lett. **109**, 112902 (2016).
[48] N. M. Dawley, E. J. Marksz, A. M. Hagerstrom, G. H. Olsen, M. E. Holtz, V. Goian, C. Kadlec, J. Zhang, X. Lu, J. A. Drisko, R. Uecker, S. Ganschow, C. J. Long, J. C. Booth, S. Kamba, C. J. Fennie, D. A. Muller, N. D. Orloff, and D. G. Schlom, Nat. Mater. **19**, 176 (2020).
[49] S. Abel, T. Stöferle, C. Marchiori, C. Rossel, M. D. Rossell, R. Erni, D. Caimi, M. Sousa, A. Chelnokov, B. J. Offrein, and J. Fompeyrine, Nat. Commun. **4**, 1671 (2013).
[50] L. Mazet, S. M. Yang, S. V. Kalinin, S. Schamm-Chardon, and C. Dubourdieu, Sci. Technol. Adv. Mater. **16**, 036005 (2015).
[51] S. Abel, F. Eltes, J. E. Ortmann, A. Messner, P. Castera, T. Wagner, D. Urbonas, A. Rosa, A. M. Gutierrez, D. Tulli, P. Ma, B. Baeuerle, A. Josten, W. Heni, D. Caimi, L. Czornomaz, A. A. Demkov, J. Leuthold, P. Sanchis, and J. Fompeyrine, Nat. Mater. **18**, 42 (2019).
[52] S. Acharya, J. Torgersen, Y. Kim, J. Park, P. Schindler, A. L. Dadlani, M. Winterkorn, S. Xu, S. P. Walch, T. Usui, C. Schildknecht, and F. B. Prinz, J. Mater. Chem. C **4**, 1945 (2016).
[53] G. Niu, G. Saint-Girons, and B. Vilquin, *Molecular Beam Epitaxy* (Elsevier, 2013), pp. 451–475.
[54] H. J. Kim, U. Kim, H. M. Kim, T. H. Kim, H. S. Mun, B.-G. Jeon, K. T. Hong, W.-J. Lee, C. Ju, K. H. Kim, and K. Char, Appl. Phys. Express **5**, 061102 (2012).
[55] J. Park, H. Paik, K. Nomoto, K. Lee, B.-E. Park, B. Grisafe, L.-C. Wang, S. Salahuddin, S. Datta, Y. Kim, D. Jena, H. G. Xing, and D. G. Schlom, APL Mater. **8**, 011110 (2020).
[56] G. H. Jonker, H. P. J. Wijn, and P. B. Braun, Philips Tech. Rev. **18**, 145 (1956-1957).
[57] P. B. Braun, Philips Res. Rep. **12**, 491–548 (1957).

© Author(s) 2020

[58]Z. Cai, T. L. Goodrich, B. Sun, Z. Chen, V. G. Harris, and K. S. Ziemer, J. Phys. D.: Appl. Phys. **43**, 095002 (2010).
[59]C. Wu, K. Kruska, and M. R. Castell, Surf. Sci. **618**, 94 (2013).
[60]R. A. McKee, F. J. Walker, J. R. Conner, E. D. Specht, and D. E. Zelmon, Appl. Phys. Lett. **59**, 782 (1991).
[61]J. Lettieri, J. H. Haeni, and D. G. Schlom, J. Vac. Sci. Technol., A **20**, 1332 (2002).
[62]Y. Segal, J. W. Reiner, A. M. Kolpak, Z. Zhang, S. Ismail-Beigi, C. H. Ahn, and F. J. Walker, Phys. Rev. Lett. **102**, 116101 (2009).
[63]K. P. Muthe, J. C. Vyas, G. P. Kothiyal, D. P. Gandhi, A. K. Debnath, S. K. Gupta, S. C. Sabharwal, and M. K. Gupta, J. Cryst. Growth **118**, 213 (1992).
[64]Y. Kado and Y. Arita, in *Extended Abstracts of the 20th (1988 International) Conference on Solid State Devices and Materials, August 24–26, 1988, Keio Plaza Hotel, Tokyo* (Publication Office, Business Center for Academic Societies Japan, Tokyo, 1988), pp. 181–184.
[65]Y. Du, D. J. Kim, T. Varga, Z. Wang, J. Szanyi, and I. Lyubinetsky, Thin Solid Films **519**, 5335 (2011).
[66]T. V. Charlu and O. J. Kleppa, J. Chem. Thermodyn. **3**, 697 (1971).
[67]M. Yano, K. Koike, M. Matsuo, T. Murayama, Y. Harada, and K. Inaba, Appl. Surf. Sci. **381**, 32 (2016).
[68]Y. Du, G. Li, E. W. Peterson, J. Zhou, X. Zhang, R. Mu, Z. Dohnálek, M. Bowden, I. Lyubinetsky, and S. A. Chambers, Nanoscale **8**, 3119 (2016).
[69]A. Radetinac, J. Zimmermann, K. Hoyer, H. Zhang, P. Komissinskiy, and L. Alff, J. Appl. Phys. **119**, 055302 (2016).
[70]P. Salg, D. Walk, L. Zeinar, A. Radetinac, L. Molina-Luna, A. Zintler, R. Jakoby, H. Maune, P. Komissinskiy, and L. Alff, APL Mater. **7**, 051107 (2019).
[71]T. M. McEvoy, K. J. Stevenson, J. T. Hupp, and X. Dang, Langmuir **19**, 4316 (2003).
[72]L. P. Borilo and E. S. Lyutova, Inorg. Mater. **53**, 400 (2017).
[73]S. I. Lopatin, I. Y. Mittova, F. S. Gerasimov, S. M. Shugurov, V. F. Kostryukov, and S. M. Skorokhodova, Russ. J. Inorg. Chem. **51**, 1646 (2006).
[74]R. A. Stall, J. Vac. Sci. Technol., B **1**, 135 (1983).
[75]G. Rispens and B. Noheda, Integr. Ferroelectr. **92**, 30 (2007).
[76]E. S. Hellman, E. H. Hartford, and R. M. Fleming, Appl. Phys. Lett. **55**, 2120 (1989).
[77]H. B. Skinner, *Mass Spectrometric Studies of Gaseous Oxides of Rhenium and of the Lanthanium Trifluoride Dimer* (U.S. Atomic Energy Commission, 1970).
[78]I. R. Beattie, T. R. Gilson, and P. J. Jones, Inorg. Chem. **35**, 1301 (1996).
[79]R. G. Behrens, R. S. Lemons, and G. M. Rosenblatt, J. Chem. Thermodyn. **6**, 457 (1974).
[80]R. F. Brebrick, J. Phase Equilib. **21**, 235 (2000).
[81]D. Manno, G. Micocci, A. Serra, and A. Tepore, J. Appl. Phys. **83**, 3541 (1998).
[82]D. Manno, G. Micocci, A. Serra, M. Di Giulio, and A. Tepore, J. Appl. Phys. **88**, 6571 (2000).
[83]W. L. Holstein, J. Phys. Chem. **97**, 4224 (1993).
[84]P. E. Blackburn, M. Hoch, and H. L. Johnston, J. Phys. Chem. **62**, 769 (1958).
[85]G. Li, T. Varga, P. Yan, Z. Wang, C. Wang, S. A. Chambers, and Y. Du, Phys. Chem. Chem. Phys. **17**, 15119 (2015).
[86]K. Sasaki, A. Kuramata, T. Masui, E. G. Víllora, K. Shimamura, and S. Yamakoshi, Appl. Phys. Express **5**, 035502 (2012).
[87]A. B. Mei, L. Miao, M. J. Wahila, G. Khalsa, Z. Wang, M. Barone, N. J. Schreiber, L. E. Noskin, H. Paik, T. E. Tiwald, Q. Zheng, R. T. Haasch, D. G. Sangiovanni, L. F. J. Piper, and D. G. Schlom, Phys. Rev. Mater. **3**, 105202 (2019).
[88]Y. Hu, J. Hwang, Y. Lee, P. Conlin, D. G. Schlom, S. Datta, and K. Cho, J. Appl. Phys. **126**, 185701 (2019).
[89]G. Hautier, A. Miglio, G. Ceder, G.-M. Rignanese, and X. Gonze, Nat. Commun. **4**, 2292 (2013).
[90]H. Okamoto, *Desk Handbook: Phase Diagram for Binary Alloys*, 2nd ed. (ASM International, 2010).
[91]*Phase Diagrams for Ceramists*, edited by R. S. Roth, J. R. Dennis, and H. F. McMurdie (American Ceramic Society, Westerville, 1987), Vol. VI.
[92]Y. Ma, A. Edgeton, H. Paik, B. D. Faeth, C. T. Parzyck, B. Pamuk, S. L. Shang, Z. K. Liu, K. M. Shen, D. G. Schlom, and C. B. Eom, Adv. Mater. **32**, 2000809 (2020).
[93]P. Vogt, F. V. E. Hensling, K. Azizie, C. S. Chang, D. Turner, J. Park, J. P. McCandless, H. Paik, B. J. Bocklund, G. Hoffman, M. Budde, O. Bierwagen, D. Jena, H. G. Xing, S. Mou, D. A. Muller, S. L. Shang, Z. K. Liu, and D. G. Schlom, "Adsorption-controlled growth of Ga_2O_3 by suboxide molecular-beam epitaxy" (unpublished).
[94]D. P. Butt, Y. Park, and T. N. Taylor, J. Nucl. Mater. **264**, 71 (1999).
[95]S. Kirklin, J. E. Saal, B. Meredig, A. Thompson, J. W. Doak, M. Aykol, S. Rühl, and C. Wolverton, npj Comput. Mater. **1**, 15010 (2015).
[96]P. Vogt and O. Bierwagen, Appl. Phys. Lett. **108**, 072101 (2016).
[97]T. Oshima, T. Okuno, and S. Fujita, Jpn. J. Appl. Phys., Part 1 **46**, 7217 (2007).
[98]M.-Y. Tsai, O. Bierwagen, M. E. White, and J. S. Speck, J. Vac. Sci. Technol., A **28**, 354 (2010).
[99]P. Vogt and O. Bierwagen, Appl. Phys. Lett. **106**, 081910 (2015).
[100]S. Krishnamoorthy, Z. Xia, S. Bajaj, M. Brenner, and S. Rajan, Appl. Phys. Express **10**, 051102 (2017).
[101]Z. Yu, C. D. Overgaard, R. Droopad, M. Passlack, and J. K. Abrokwah, Appl. Phys. Lett. **82**, 2978 (2003).
[102]S. Ghose, S. Rahman, L. Hong, J. S. Rojas-Ramirez, H. Jin, K. Park, R. Klie, and R. Droopad, J. Appl. Phys. **122**, 095302 (2017).
[103]A. Sudha, T. K. Maity, S. L. Sharma, and A. N. Gupta, Mater. Sci. Semicond. Process. **74**, 347 (2018).
[104]M. D. Losego, *Interfacing Epitaxial Oxides to Gallium Nitride* (North Carolina State University, 2008).
[105]A. Schmehl, V. Vaithyanathan, A. Herrnberger, S. Thiel, C. Richter, M. Liberati, T. Heeg, M. Röckerath, L. F. Kourkoutis, S. Mühlbauer, P. Böni, D. A. Muller, Y. Barash, J. Schubert, Y. Idzerda, J. Mannhart, and D. G. Schlom, Nat. Mater. **6**, 882 (2007).
[106]R. Sutarto, S. G. Altendorf, B. Coloru, M. Moretti Sala, T. Haupricht, C. F. Chang, Z. Hu, C. Schüßler-Langeheine, N. Hollmann, H. Kierspel, H. H. Hsieh, H.-J. Lin, C. T. Chen, and L. H. Tjeng, Phys. Rev. B **79**, 205318 (2009).
[107]D. V. Averyanov, O. E. Parfenov, A. M. Tokmachev, I. A. Karateev, O. A. Kondratev, A. N. Taldenkov, M. S. Platunov, F. Wilhelm, A. Rogalev, and V. G. Storchak, Nanotechnology **29**, 195706 (2018).
[108]O. Bierwagen, A. Proessdorf, M. Niehle, F. Grosse, A. Trampert, and M. Klingsporn, Cryst. Growth Des. **13**, 3645 (2013).
[109]J. Wang, T. Ji, Y. Zhu, Z. Fang, and W. Ren, J. Rare Earths **30**, 233 (2012).
[110]K. J. Hubbard and D. G. Schlom, J. Mater. Res. **11**, 2757 (1996).
[111]D. G. Schlom and J. H. Haeni, MRS Bull. **27**, 198 (2002).
[112]D. G. Schlom, S. Guha, and S. Datta, MRS Bull. **33**, 1017 (2008).
[113]C. P. Chen, M. Hong, J. Kwo, H. M. Cheng, Y. L. Huang, S. Y. Lin, J. Chi, H. Y. Lee, Y. F. Hsieh, and J. P. Mannaerts, J. Cryst. Growth **278**, 638 (2005).
[114]J. Kwo, M. Hong, A. R. Kortan, K. L. Queeney, Y. J. Chabal, R. L. Opila, D. A. Muller, S. N. G. Chu, B. J. Sapjeta, T. S. Lay, J. P. Mannaerts, T. Boone, H. W. Krautter, J. J. Krajewski, A. M. Sergnt, and J. M. Rosamilia, J. Appl. Phys. **89**, 3920 (2001).
[115]J. P. Liu, P. Zaumseil, E. Bugiel, and H. J. Osten, Appl. Phys. Lett. **79**, 671 (2001).
[116]T. Watahiki, W. Braun, and H. Riechert, J. Vac. Sci. Technol., B **27**, 262 (2009).
[117]A. Fissel, Z. Elassar, O. Kirfel, E. Bugiel, M. Czernohorsky, and H. J. Osten, J. Appl. Phys. **99**, 074105 (2006).
[118]M. Czernohorsky, E. Bugiel, H. J. Osten, A. Fissel, and O. Kirfel, Appl. Phys. Lett. **88**, 152905 (2006).
[119]G.-Y. Adachi and N. Imanaka, Chem. Rev. **98**, 1479 (1998).
[120]W. Braun and J. Mannhart, AIP Adv. **9**, 085310 (2019).
[121]V. L. Stolyarova, A. L. Shilov, G. G. Ivanov, M. M. Shultz, and S. Seetharaman, Rapid Commun. Mass Spectrom. **9**, 1244 (1995).
[122]J. H. Lee, L. Fang, E. Vlahos, X. Ke, Y. W. Jung, L. F. Kourkoutis, J.-W. Kim, P. J. Ryan, T. Heeg, M. Roeckerath, V. Goian, M. Bernhagen, R. Uecker, P. C. Hammel, K. M. Rabe, S. Kamba, J. Schubert, J. W. Freeland, D. A. Muller, C. J. Fennie, P. Schiffer, V. Gopalan, E. Johnston-Halperin, and D. G. Schlom, Nature **466**, 954 (2010).
[123]A. P. Mackenzie and Y. Maeno, Rev. Mod. Phys. **75**, 657 (2003).

© Author(s) 2020

[124]S. A. Grigera, Science **306**, 1154 (2004).
[125]Y. K. Kim, N. H. Sung, J. D. Denlinger, and B. J. Kim, Nat. Phys. **12**, 37 (2016).
[126]Y. Singh, S. Manni, J. Reuther, T. Berlijn, R. Thomale, W. Ku, S. Trebst, and P. Gegenwart, Phys. Rev. Lett. **108**, 127203 (2012).
[127]X. Wan, A. M. Turner, A. Vishwanath, and S. Y. Savrasov, Phys. Rev. B **83**, 205101 (2011).
[128]L. Miao, Y. Lee, A. B. Mei, M. J. Lawler, and K. M. Shen, Nat. Commun. **11**, 1341 (2020).
[129]D.-Y. Kuo, J. K. Kawasaki, J. N. Nelson, J. Kloppenburg, G. Hautier, K. M. Shen, D. G. Schlom, and J. Suntivich, J. Am. Chem. Soc. **139**, 3473 (2017).
[130]D.-Y. Kuo, H. Paik, J. Kloppenburg, B. Faeth, K. M. Shen, D. G. Schlom, G. Hautier, and J. Suntivich, J. Am. Chem. Soc. **140**, 017597 (2018).
[131]D. Klimm, S. Ganschow, D. Schulz, R. Bertram, R. Uecker, P. Reiche, and R. Fornari, J. Cryst. Growth **311**, 534 (2009).
[132]C. Mallika and O. M. Sreedharan, J. Less-Common Met. **162**, 51 (1990).
[133]L. E. Noskin, A. Seidner H., and D. G. Schlom, MRS Adv. **2**, 3031 (2017).

© Author(s) 2020